Characterization of biogenic volatile organic compounds and their oxidation products at a stressed spruce-dominated forest close to a biogas power plant

Junwei Song[1,4,*], Georgios I. Gkatzelis[2], Ralf Tillmann[2], Nicolas Brüggemann[3], Thomas Leisner[1] and Harald Saathoff[1,*]

[1] Institute of Meteorology and Climate Research, Karlsruhe Institute of Technology, Hermann-von-Helmholtz-Platz 1, 76344 Eggenstein-Leopoldshafen, Germany

[2] Institute of Energy and Climate Research, IEK-8: Troposphere, Forschungszentrum Jülich GmbH, 52425 Jülich, Germany

[3] Institute of Bio- and Geosciences, IBG-3: Agrosphere, Forschungszentrum Jülich GmbH, 52425 Jülich, Germany

[4] Université Claude Bernard Lyon 1, CNRS, IRCELYON, UMR 5256, F-69626, Villeurbanne, France

Correspondence: Junwei Song (junwei.song@ircelyon.univ-lyon1.fr) and Harald Saathoff (harald.saathoff@kit.edu)

Abstract

Biogenic volatile organic compounds (BVOCs) are key components of the atmosphere, playing a significant role in the formation of organic aerosols (OA). However, only few studies have simultaneously examined the characteristics of BVOCs and OA in the forest under the impact of consecutive droughts and extensive bark beetle infestations. Here we present real-time measurements of OA and BVOCs at a stressed Norway spruce-dominated forest near a biogas power plant (BPP) in western Germany during June 2020. A proton-transfer-reaction time-of-flight mass spectrometer coupled with a particle inlet (CHARON-PTR-ToF-MS) and a Vocus-PTR-ToF-MS were used to measure OA and BVOCs. The average mass concentration of OA was 0.8 ± 0.5 µg m^{-3}, consisting mainly of semi-volatile monoterpene oxidation products. The average mixing ratios of isoprene (0.58 ± 0.54 ppb) and monoterpenes (2.5 ± 5.3 ppb) were higher than the values previously measured in both German temperate forests and boreal forests. Based on wind direction analysis, BVOC data were categorized into two groups with one mainly influenced by the biogenic emissions from an intact forest and a clear-cut area (biogenic-group) and another one by the anthropogenic emissions from a BPP and a village (anthropogenic-group). High mixing ratios of monoterpenes were observed in the anthropogenic-group, indicating a significant contribution of BPP emissions. In the biogenic-group, the variations of BVOC mixing ratios were driven by the interplay between meteorology, biogenic emissions and their photochemical consumption. Positive matrix factorization analysis of VOCs revealed substantial contributions of oxygenated organic compounds from the photochemical oxidation of BVOCs during daytime, while monoterpenes and their weakly oxidized products dominated at night. Furthermore, increasing relative humidity and decreasing temperatures promoted the gas-to-particle partitioning of these weakly oxidized monoterpene products, leading to an increase in nighttime OA mass. The results demonstrate the variations of BVOCs are influenced not only by meteorological conditions and biogenic emissions but also by local BPP emissions and subsequent chemical transformation processes. This study highlights the need to investigate the changes of biogenic emissions in European stressed forests.

1 Introduction

Volatile organic compounds (VOCs) play important roles in determining atmospheric chemical processes (Atkinson, 2000; Hallquist et al., 2009; Yáñez-Serrano et al., 2020; Shrivastava et al., 2017; Rasmussen and Went, 1965; Trainer et al., 1987; Peñuelas and Staudt,

2010). Terrestrial ecosystems emit large amounts of biogenic VOCs (BVOCs, >1000 Tg yr^{-1}) to the global atmosphere, more than anthropogenic VOCs (AVOCs, ~200 Tg yr^{-1}) (Guenther et al., 2012; Sindelarova et al., 2014). BVOCs emitted by vegetation consist largely of reactive terpenoids e.g., isoprene (~70%), monoterpenes (~11%) and sesquiterpenes (~2.5%) (Sindelarova et al., 2014). The oxidation products of terpenoids can nucleate to form new particles or contribute to the growth of existing particles and secondary organic aerosol (SOA) formation, thus impacting air quality and climate (Hallquist et al., 2009; Shrivastava et al., 2017).

Over the last decade, many field studies have been conducted at different forest ecosystems to investigate the characteristics of BVOCs including the emissions, temporal variations as well as their impacts on atmospheric reactivity and SOA formation (Hakola et al., 2012; Hellén et al., 2018; Li et al., 2020; Huang et al., 2021; Yáñez-Serrano et al., 2021; Vestenius et al., 2021; Mermet et al., 2021; Vermeuel et al., 2023; Weber et al., 2022; Bourtsoukidis et al., 2024; Bourtsoukidis et al., 2014). The diurnal pattern of isoprene concentrations in forests shows typically higher values during daytime (Yáñez-Serrano et al., 2021; Li et al., 2020; Hakola et al., 2012), since isoprene emissions increase with temperature and sunlight intensity as result of increased de-novo production and direct release. In contrast, monoterpenes are mainly released from storage pools of boreal pines. The emissions and composition of BVOCs from trees varies with abiotic and biotic stresses such as high temperature (Teskey et al., 2015; Kleist et al., 2012), drought (Peron et al., 2021; Bonn et al., 2019) and herbivore attack (Jaakkola et al., 2023; Kari et al., 2019; Faiola and Taipale, 2020). It has been reported that these stresses can alter the emissions of BVOCs, especially of terpenoids (Ghimire et al., 2016; Jaakkola et al., 2023; Byron et al., 2022).

In addition to biogenic emissions, the temporal variations of BVOC concentrations especially of terpenoids are influenced by atmospheric oxidation processes. The diurnal variation of monoterpene concentrations shows lower values during daytime than nighttime in the boreal forests, which were attributed to the rapid photochemical consumption and expanded boundary layer heights (Hellén et al., 2018; Hakola et al., 2012). Correspondingly, higher concentrations of monoterpene oxidation products are expected to be produced during daytime. For instance, Huang et al., (2021) found that some gaseous monoterpene oxidation products e.g., $C_7H_{10}O_4$ (3,6-oxoheptanoic acid) and $C_8H_{12}O_4$ (terpenylic acid) showed higher concentrations during daytime in a boreal forest. Li et at., (2020) reported similar diurnal variations of gaseous higher-oxidized monoterpene products (e.g., $C_8H_{12}O_{4\text{-}6}$, $C_9H_{14}O_{4\text{-}6}$, $C_{10}H_{14}O_{4\text{-}6}$ and $C_{10}H_{16}O_{4\text{-}6}$) in the French Landes-forest largely composed of maritime pines.

The variations of BVOC oxidation products are also influenced by gas-particle partitioning processes. Laboratory studies have shown that decreasing temperature and increasing relative humidity (RH) can lead to an increased particulate fraction of SOA products from BVOC oxidation (Surdu et al., 2023; Von Hessberg et al., 2009; Tillmann et al., 2010; Zhang et al., 2015; Luo et al., 2024). However, due to lack of online dual-phase measurements only few field studies have focused on the gas-particle partitioning of BVOC oxidation products in the healthy forests (Mohr et al., 2017; Yatavelli et al., 2014; Isaacman-Vanwertz et al., 2016; Lee et al., 2018). However, our understanding of the interplay between gas and particle phases of BVOC oxidation products in real forest atmosphere, particularly in stressed forest, remains limited. Addressing these gaps is crucial for assessing the impact of various environmental factors on BVOC emissions and their subsequent transformation (Faiola and Taipale, 2020).

The Eifel is a low mountain range in western Germany that stretches across the federal states of North Rhine-Westphalia and Rhineland-Palatinate and covers an area of ~5300 km^2. Its forested areas are largely composed of Norway spruce (*Picea abies* (L.) Karst.), which are important contributors to BVOCs (Smiatek and Steinbrecher, 2006; Kleist et al., 2012). The Eifel Forest was suffering from severe droughts, heatwaves and bark beetle infestation in the years before our measurements, thus it can serve as a case for examining the variations of BVOCs in a stressed European coniferous forest. In this study, a field measurement campaign was conducted at a site of the northern Eifel Forest in the vicinity of a biogas power plant (BPP). Europe is the world leader in biogas electricity production with more than 18,000 BPPs (Brémond et al., 2021). These BPPs are widely distributed in European rural areas close to the forest region (Bakkaloglu et al., 2021; Scheftelowitz et al., 2018), which emit large amounts of CH_4 and VOCs periodically to the atmosphere around the BPPs (Salazar Gómez et al., 2016). In this paper, we present the real-time measurements of VOCs and aerosol particles measured by a proton-transfer-reaction time-of-flight mass spectrometer (PTR-ToF-MS) coupled with a particle inlet (CHARON, chemical analysis of aerosol online) and a Vocus-PTR-ToF-MS. The impacts of meteorological conditions, sources and chemical oxidation processes on the variations of BVOCs and their gaseous and particulate oxidation products were investigated to get a better understanding of BVOC emissions and their contributions to SOA as well as the potential impact of BPP emissions.

2 Methods

2.1 Sampling site

In In this study, a three-week field campaign was conducted at a site in the northern Eifel Forest (50.72° N, 6.40° E) during June 2020 as a part of the "Heat and Drought 2020" campaign of the Modular Observation Solutions of Earth Systems (MOSES) project of the Helmholtz Association of German Research Centers. The Eifel Forest was suffering from severe droughts, heatwaves and severe bark beetle infestation in the last years (Weber et al., 2022b; Ghimire et al., 2016). Within two years (2018-2020), 14% of the spruce in the Northern Eifel region were removed due to summer droughts and only 28.3% remained in good condition (Montzka et al., 2021). Therefore, the Eifel Forest can serve as an example of a stressed temperate coniferous forest.

As shown in **Fig. 1**, the measurement site is situated directly next to a stand of Norway spruce with a few shrubs and blueberry plants also surrounding the area. To the south and southeast of the measurements site, there were some clear-cut areas due to bark beetle infestation in the years of 2018-2020. Additionally, the measurement site was located ~400 m southeast of a football field in the small village Kleinhau belonging to the municipality of Hürtgenwald, Germany (population about 9000) and ~250 m east of a BPP (BioEnergie Kleinhau GmbH). The biomass substrate used for the biogas production in this BPP consisted mainly of crop waste (e.g., corn stover). The measurement site was affected by the BPP emissions especially for westerly wind directions.

2.2 Instrumentation

All instruments were set up in a temperature-controlled measurement container (~25 °C) located at the sampling site. All sampling inlets were located 3.7 m above ground level and 1 m above the container roof. An overview of instruments and parameters measured is given in **Table S1**.

A PTR-ToF-MS 4000X2 coupled with a CHARON particle inlet (Ionicon Analytik GmbH, Innsbruck, Austria) was deployed to measure the VOCs and aerosol particles from 5th-30th of June 2020. A detailed description of the PTR-ToF-MS and CHARON inlet has been provided elsewhere (Jordan et al., 2009; Muller et al., 2017; Eichler et al., 2015). Briefly, CHARON consists of a charcoal denuder for stripping off gaseous organics, an aerodynamic lens for enriching particles, and a thermo-desorption unit for particle evaporation prior to chemical analysis by PTR-ToF-MS. In this campaign, both gases and particles were measured through alternatingly switching between different modes with the data acquisition software (IoniTOF

4.0, Ionicon Analytik GmbH, Innsbruck, Austria). Specifically, one alternating measurement cycle includes 3-min HEPA filter mode for measuring the particle background, 1-min transition mode for the instrument equilibrium, 10-min CHARON mode for measuring particle phase compounds, another 1-min transition mode and 10-min VOC mode for measuring gas phase compounds (**Fig. S1**). One minute transition time is sufficient for the equilibrium of instrumental conditions between different modes (Piel et al., 2021). During the gas-phase measurement, ambient air was sampled continuously from a 3 m long perfluoroalkoxy tube (1/4 inch inner diameter) with a total flowrate of 1.45 L min^{-1}, and then a subset flow of ~0.1 L min^{-1} was sampled by the PTR-MS through a polyetheretherketone tubing maintained at 80 °C. During the particle-phase measurement, ambient particles were sampled by a $PM_{2.5}$ inlet with a flowrate of 16.7 L min^{-1}, out of which a flow of 0.55 L min^{-1} was directed to the CHARON inlet maintained by a vacuum pump (ACP15, Pfeiffer Vacuum). During a first measurement stage from 5^{th}-19^{th} of June, the PTR drift tube was set with alternating temperatures for gas and particle phase measurement modes at 80 °C and 120 °C respectively. With this setting, the actual drift tube temperatures were varying during the gas and particle measurement modes complicating the data analysis (**Figs. S1 and S2**). During a second measurement stage from 22^{nd}-30^{th} of June, the PTR drift tube was set with the same temperature of 120 °C and a drift tube pressure of 2.7 mbar for both gas and particle measurement modes. The CHARON inlet was set to a thermo-desorption unit temperature of 150 °C and a pressure of 7-8 mbar. Finally, the electric field (E/N) of the CHARON-PTR-TOF-MS was kept at ~97 Td and ~57 Td for the gas and particle phase measurement modes respectively during the second measurement stage. Please note that during the first measurement stage the actual temperature of the drift tube fluctuated and was lower than the intended temperature of 120 °C (**Fig. S1**). This made it difficult to quantify organic compounds in the particle phase measured by the CHARON-PTR-ToF-MS. For the gas phase measurements, we corrected the major VOC data from the first measurement stage based on the gas calibration and the cross-comparison with Vocus-PTR-ToF-MS measurements. Consequently, we can present the major VOC species measured by the CHARON-PTR-ToF-MS for the entire campaign, while the particle phase data for first measurement stage were excluded for further analysis in this study.

Gas calibrations of CHARON-PTR-TOF-MS were performed via dynamic dilution of a calibration gas cylinder containing 11 VOC species (**Table S2**, accuracy 10% at ~100 ppb). The background of VOCs was taken from zero-air measurements during the gas calibrations at the beginning and the end of the campaign. The enrichment factor of the CHARON inlet was determined using an external calibration with size-selected ammonium nitrate particles

(NH_4NO_3) that were counted using a condensation particle counter (CPC3772, TSI Inc., Shoreview, MN, USA). The enrichment factor was determined with an average value of 18 ± 2 in the 150-700 nm particle size range, with lower values for smaller particles below 150 nm (**Fig. S3**). The particle background was determined by a high-efficiency HEPA filter (ETA filter model HC01-5N-B, Aerocolloid LLC, Minneapolis, MN, USA) that was placed upstream of the gas-phase denuder of the CHARON inlet. All data files recorded by the CHARON-PTR-ToF-MS were processed by the software IONICON Data Analyzer (IDA version1.0.0.2, Ionicon Analytik GmbH, Innsbruck, Austria). More details of data processing with the IDA are given in **Supplement S1**.

A Vocus-PTR-ToF-MS (Aerodyne Research Inc., Billerica, MA, USA) was deployed to measure VOCs and oxygenated VOCs concurrently with the CHARON-PTR-ToF-MS from 10^{th}-30^{th} of June. The Vocus-PTR-ToF-MS was not available for measurements before 10^{th} June 2020 due to a technical problem. The details of the Vocus-PTR-ToF-MS have been described elsewhere (Krechmer et al., 2018). The Vocus-PTR-ToF-MS is characterized by a newly designed reagent-ion source and a focusing ion-molecule reactor (FIMR), both of which improve the detection efficiency of ions. In this study, the FIMR was operated at a pressure of 1.5 mbar. The mass resolving power of the Vocus mass analyzer was ~10000 amu/Δamu. Raw data were recorded with a time resolution of 5 s. For the Vocus-PTR-ToF-MS measurement, ambient air was drawn in through a 1 m long PFA tubing with a total flow rate of 4.5 L min^{-1}, and then a subset flow of 0.1-0.15 L min^{-1} went into the Vocus-PTR-ToF-MS. Background measurements using high-purity nitrogen were automatically performed every hour. The Vocus-PTR-ToF-MS was regularly calibrated using a home-made gas standard of 15 compounds at ~1 ppmv with accuracy of 10% (**Table S2**). At the end of the campaign, a gas cross calibration was performed between Vocus-PTR-ToF-MS and CHARON-PTR-ToF-MS with the calibration gas cylinder (Ionicon Analytik GmbH). The Vocus-PTR-ToF-MS data analysis was performed using the software package "TOFware" (AG, Thun, Switzerland). For the quantification of uncalibrated species measured by the Vocus-PTR-ToF-MS, we adopted the rate constants of proton transfer reactions (K_{cap}) from the PTR library (Pagonis et al., 2019). We then generated a sensitivity for the uncalibrated masses by applying a correction factor based on the k_{cap} ratios to the calibrated masses. Finally, the Vocus-PTR-ToF-MS data were synchronized to the measurement time of CHARON-PTR-ToF-MS for comparison of the VOC data. In this study, a series of VOC species were simultaneously detected by the CHARON-PTR-ToF-MS and the Vocus-PTR-ToF-MS with a detailed comparison provided in **Supplement S2**.

In addition, methane (CH_4), carbon dioxide (CO_2), water vapor (H_2O) and carbon monoxide (CO) were measured with a cavity ring-down spectrometer (G2401; Picarro, Santa Clara, CA, USA) from 10^{th}-30^{th} of June. O_3 was measured by a commercial chemiluminescence analyzer (Cranox II, Eco Physics GmbH, Hürth, Germany). An optical particle counter (OPC, Fidas200, Palas, Karlsruhe, Germnay) was used to measure the mass concentrations of $PM_{2.5}$ and PM_{10} from 5^{th}-30^{th} of June. Simultaneously, black carbon (BC) concentrations were measured with an aethalometer (MA200, AethLabs, CA, USA). Particle number concentrations were measured with a condensation particle counter (CPC3776, TSI Inc., Shoreview, MN, USA). A nanoparticle sizer (NanoScan SMPS, TSI3910, TSI Inc., Shoreview, MN, USA) was used to measure the particle number size distribution between 10-410 nm.

Meteorological parameters were measured by a compact sensor (WS700, Lufft GmbH, Fellbach, Germany). The meteorological data were missing during some short periods due to the malfunction of data acquisition. We also used hourly data of temperature, relative humidity (RH), precipitation, and planetary boundary layer (PBL) height from the European Centre for Medium-Range Weather Forecasts ERA5 reanalysis (Hersbach et al., 2020), as well as wind speed and direction data form NASA Power Data Access Viewer (power.larc.nasa.gov) to complement the meteorological data. The daily soil moisture was measured by a Cosmic-Ray Neutron Sensor (CRNS) (Bogena et al., 2015), which was located ~150 m southwest of the sampling site. In addition, the spatial distribution of soil moisture in the northern Eifel Forest was determined from the measurement of a CRNS rover.

2.3 Positive matrix factorization analysis

The PMF receptor model is a bilinear analytic algorithm that separates the time series of air pollutants to different sources represented by factor profiles, factor time series and residual signals (Paatero and Tapper, 1994). The PMF model has been widely used to determine different sources and chemical processes of VOCs measured by the PTR-ToF-MS in the urban, rural and forest atmospheres (Gkatzelis et al., 2021; Li et al., 2021a; Wang et al., 2020; Li et al., 2022; Pernov et al., 2021; Desservettaz et al., 2023; Jain et al., 2023; Song et al., 2024). To explore the sources and chemical processes of VOCs, we performed the PMF analysis of VOC species measured by the Vocus-PTR-ToF-MS rather than those measured by CHARON-PTR-ToF-MS. This is mainly due to the Vocus-PTR-ToF-MS can measure higher molecular weight OVOCs (*mz*> 200) well that provides more information for interpreting the oxidation processes of BVOCs (Li et al., 2021a).

In this study, the Vocus-PTR-ToF-MS-measured VOC ions with a chemical formula assignment (mainly $C_xH_y^+$ and $C_xH_yO_z^+$) were selected to perform the PMF analysis. The PMF input data was prepared according to the protocol reported in previous studies (Pernov et al., 2021; Li et al., 2022). The uncertainties were calculated with the following equations:

$$Unc. = \begin{cases} LOD \times \frac{5}{6} & conc \le LOD \quad (1) \\ \sqrt{LOD^2 + (Error\ fraction \times conc.)^2} & conc. > LOD \quad (2) \end{cases}$$

where the concentrations of a VOC ion below the limit of detection (LOD) were replaced with half of the LOD and the associated uncertainties were set to 5/6 of the LOD using the Equation 1. The uncertainties of a VOC ion above the LOD were calculated using the Equation 2, assuming an error fraction of 10%. We excluded the VOC species from the PMF analysis if their concentration data are significantly below LOD (> 20%) during the entire measurement campaign. For example, we excluded the signal of $C_4H_9^+$ for PMF analysis because its signals were mostly below the LOD during a significant fraction of the measurement period (**Fig. S4**). Finally, 157 VOC ions were selected for the PMF analysis (**Table S3**). The sum mixing ratios of these 157 VOC ions measured by the Vocus-PTR-ToF-MS showed a good agreement with the sum mixing ratios of 112 major VOC ions simultaneously measured by the CHARON-PTR-ToF-MS (**Fig. S4**). Therefore, the solution of PMF analysis on these 157 VOC ions measured by the Vocus-PTR-ToF-MS can reasonably interpret the major sources and/or chemical processes of VOCs in this study. The PMF analysis was performed using the PMF Evaluation Tool (v3.05) that runs in IGOR Pro software (v6.37, Wavemetrics, Portland, OR). The optimal PMF solution was explored across several solution diagnostics of factors ranging 1 to 10. The 6-factor solution was chosen as the optimal and interpretable solution. After 6 factors, increasing the factor number will cause the factor splitting and provide uninterpretable results (**Fig. S5**). The summary of diagnostic plots for the 6-factor solution is given in **Fig. S6**.

2.4 Calculation of particle-phase fraction of organic compounds

To estimate the gas-to-particle partitioning processes, we calculated the particulate mass fraction (F_p) of organic compounds by the Equation 3:

$$F_p = \frac{C_{p,i}}{C_{g,i}+C_{p,i}} \quad (3)$$

where $C_{p,i}$ and $C_{g,i}$ are the particle and gas phase concentrations of the individual organic compound measured by CHARON-PTR-ToF-MS and Vocus-PTR-ToF-MS, respectively.

3 Results and discussion

In the first section we will give an overview of the measurements conducted and in the second section we will address the impacts of meteorological factors like wind speed and direction, temperature, and relative humidity on the variations of gas and particle concentrations. In the third section we perform a source apportionment of the VOCs observed, and in the last section we discuss BVOC oxidation products in gas and particle phase.

3.1 Overview of the measurements

3.1.1 Meteorology

During the entire measurement campaign, the ambient temperature ranged from 6.8 to 30.8 °C with an average of 16.6 ± 4.7 °C, and the relative humidity (RH) varied from 31% to 98% with an average of 71% ± 16% respectively (**Fig. 2**). The wind speeds ranged from 0-5.5 m s^{-1} with an average of 1.3 ± 0.9 m s^{-1}. Wind directions varied significantly during the entire measurement period. The sampling site was potentially affected by BPP-related and/or anthropogenic emissions depending on the wind directions (**Fig. 1**). The leaf area index of the Eifel Forest during our measurement period was determined to be ~2.5 ± 0.02 m^2 m^{-2} based on the ERA5 reanalysis data. The soil moisture was measured to be 0.3 ± 0.04 m^3 m^{-3} at a station located ~150 m southwest of the sampling site. In addition, the spatial distribution of soil moisture in the northern Eifel Forest also showed low values (<0.3 m^3 m^{-3}) in most areas covering our sampling site (**Fig. S7**). Therefore, the Eifel Forest was under relatively dry condition during our measurement period.

During the entire measurement campaign, we observed two characteristic episodes, Episode 1 (0:00 9th of June to 0:00 12th of June) and Episode 2 (12:00 23rd of June to12:00 26th of June), for different meteorological conditions. During Episode 1, the daily maximum temperature remained below 20 ºC for three consecutive measurement days. During Episode 2, the daily maximum temperature exceeded 25 ºC for three consecutive measurement days. Therefore, hereafter we define these two episodes as low-T and high-T episodes, respectively. Both episodes had very low wind speeds (< 1 m s^{-1}), suggesting the site was influenced by local emissions and chemical transformation or aging processes. The impacts of meteorology and chemical processes on the variations of gases and particles will be discussed in the following sections.

3.1.2 Mixing ratios of gas species

As shown in **Fig. 3**, the average mixing ratios of CO and CO_2 were 0.11 ± 0.02 ppm and 410 ± 1 ppm respectively from 10^{th}-30^{th} of June. The mixing ratios of CH_4 ranged from 1.90 to 2.56 ppm with an average of 1.98 ± 0.05 ppm. Spikes of CH_4 (> 2.2 ppm) were occasionally observed during the days of 17, 20-21 and 23 June, which are associated with BPP-related emissions as validated in Section 3.2. Isoprene and monoterpenes were quantitatively measured by the CHARON-PTR-ToF-MS and Vocus-PTR-ToF-MS with good to fair correlations (r = 0.92 and 0.59 for isoprene and monoterpenes, respectively). During the entire campaign, the average mixing ratios of isoprene was 0.58 ± 0.54 ppb, slightly higher than that previously reported in a Norway spruce-dominated forest (0.32 ± 0.17 ppb) in central Germany (Bourtsoukidis et al., 2014) and a mixed-conifer forest (max. 0.25 ppb) with Norway spruce and Scots pine (*Pinus sylvestris* L.) in Sweden (Petersen et al., 2023). The level of isoprene in this study was comparable to that (~0.6 ppb) observed in French Landes forest dominated by maritime pine trees (*Pinus pinaster* Aiton) during summer time (Li et al., 2020), but higher than those (0.01-0.2 ppb) reported for the boreal forests in Finland dominated by Scots pine (Li et al., 2021a; Hellén et al., 2018). The average mixing ratios of monoterpenes (2.5 ± 5.3 ppb) in this study was also higher than that reported in a Norway spruce-dominated forest (0.50 ± 0.21 ppb) in central Germany (Bourtsoukidis et al., 2014), but lower than that observed in the French Landes forest (~6 ppb) (Li et al., 2020). Relatively low mixing ratios of monoterpenes were reported previously for the boreal forests in Finland (~0.8 ppb) during summertime (Li et al., 2020; Mermet et al., 2021). Note that monoterpenes had a significant concentration variation in this study, which is attributed to the occurrence of monoterpene spikes (**Fig. 3d**). These monoterpene spikes were mainly related to the impact of BPP-related emissions as discussed in section 3.2. In this study, the average mixing ratios of sesquiterpenes measured by the CHARON-PTR-ToF-MS was 0.01 ± 0.01 ppb, a factor of two higher than that measured by the Vocus-PTR-ToF-MS. The average mixing ratios of sesquiterpenes was lower than that measured by a Vocus-PTR-ToF-MS in the French Landes forest (~0.06 ppb) (Li et al., 2020). It should be noted that the quantification of sesquiterpenes is affected by the degree of sesquiterpene fragmentation inside the PTR-ToF-MS, which can vary significantly depending on the instrument setting (Kim et al., 2009; Kari et al., 2018). In addition, sesquiterpenes may experience wall losses inside the inlet tubing and the instrument, and have low transmissions (Li et al., 2020). Due to a lack of a dedicated sesquiterpene calibration in this study, the quantification of sesquiterpenes measured by the PTR-ToF-MS can be regarded as the lower limit without the consideration of fragmentation.

3.1.3 Chemical composition of aerosol particles

During the entire campaign, the average mass concentrations of $PM_{2.5}$ and BC were 5.5 ± 4.7 μg m^{-3} and 0.2 ± 0.1 μg m^{-3} respectively (**Fig. S8**). The aerosol particle composition including organic aerosol (OA), nitrate, and ammonium measured by the CHARON-PTR-ToF-MS and BC by the aethalometer are simultaneously available from 22nd-30th of June (**Fig. 4**). During this period, the average mass concentrations of OA was 0.8 ± 0.5 μg m^{-3}, accounting for 15 ± 6 % of $PM_{2.5}$ mass. The mass fraction of CHARON-PTR-ToF-MS-measured OA in $PM_{2.5}$ was close to that of semi-volatile oxygenated organic aerosol in $PM_{2.5}$ (9%-13%) resolved from the PMF analysis of OA measured by an aerosol mass spectrometer (AMS) in urban and rural environments (Song et al., 2022; Huang et al., 2019). The elemental ratios of OA (O:C and H:C) measured by the CHARON-PTR-ToF-MS were 0.32 ± 0.03 and 1.56 ± 0.10, respectively, which are comparable to the values of semi-volatile oxygenated organic aerosol (O:C: 0.35 ± 0.14 and H:C: 1.55 ± 0.10) resolved from the AMS-PMF analysis in previous studies (Ng et al., 2011; Ng et al., 2010). These results indicate that the OA mass detected by the CHARON-PTR-ToF-MS is mainly composed of semi-volatile organic compounds in this study. Please note that the fragmentation of organic compounds in the CHARON-PTR-ToF-MS may result in low average O:C values of bulk OA compared to those measured by the AMS (Leglise et al., 2019).

Mass concentrations of OA associated with individual *m/z* signals detected by the CHARON-PTR-ToF-MS ranged from ~0.1 to ~65 ng m^{-3}. In total, 164 organic ions can be well assigned with the chemical formula of $C_xH_y^+$ or $C_xH_yO_z^+$, contributing to 67 ± 11 % of total OA mass measured by the CHARON-PTR-ToF-MS. Furthermore, the organic ions assigned were mainly distributed in the C_2-C_{10} range with oxygen atom numbers of 0-5 (**Fig. 4d**). Müller et al., (2017) observed a similar mass distribution of OA measured by the CHARON-PTR-ToF-MS in Valencia, Spain which was associated with the oxidation of abundant monoterpenes emitted from trees. With the same instrument, Gkatzelis et al., (2018) also reported a similar chemical composition of OA from the oxidation of tree emissions dominated by α-pinene and β-pinene in simulation chamber experiments. The abundant species in the C_2-C_8 range (**Fig. 4d**) are most likely fragments from $C_{9\text{-}10}$-monoterpene derived oxidized products which are prone to fragmentation in the CHARON-PTR-ToF-MS (Gkatzelis et al., 2018). Leglise et al., (2019) and Peng et al., (2023) further confirm the fragmentation of oxygenated organic compounds inside the CHARON-PTR-ToF-MS via the loss of neutral water, carbonyl, or carboxyl groups (-H_2O, -CO and -CO_2). For instance, *cis*-pinonic acid ($C_{10}H_{17}O_3^+$) a monoterpene oxidation

product as detected by the CHARON-PTR-ToF-MS can produce the typical fragment ions of $C_4H_7O^+$, $C_6H_{11}O_2$+ and $C_{10}H_{15}O_2^+$ (Peng et al., 2023; Leglise et al., 2019). Furthermore, the relative abundance of fragment ions ($C_4H_7O^+$, $C_6H_{11}O_2$+ and $C_{10}H_{15}O_2^+$) were generally higher than the parent ion $C_{10}H_{17}O_3^+$ (Leglise et al., 2019; Peng et al., 2023). In this study, we found that only a small fraction of the *cis*-pinonic acid parent ion $C_{10}H_{17}O_3^+$ was detected by the CHARON-PTR-ToF-MS compared to the fragment ions $C_4H_7O^+$, $C_6H_{11}O_2^+$ and $C_{10}H_{15}O_2^+$. Similarly, other monoterpene oxidation products such as $C_9H_{15}O_3^+$ (e.g., norpinonic acid) and $C_8H_{13}O_4^+$ (e.g., norpinic acid) showed lower abundances at their parent ions compared to their fragment ions with one H_2O molecule lost ($C_9H_{13}O_2^+$ and $C_8H_{11}O_3^+$) (**Fig. S9**). We observed good correlations between $C_9H_{15}O_3^+$ and $C_9H_{13}O_2^+$ (r = 0.73), as well as between $C_8H_{13}O_4^+$ and $C_8H_{11}O_3^+$ (r =0.97), indicating that $C_9H_{13}O_2^+$ and $C_8H_{11}O_3^+$ are fragment ions from parent compounds. Previous studies have shown that the fragmentation pattern of oxidized organic compounds in the CHARON-PTR-ToF-MS varied depending on the instrument settings (Leglise et al., 2019; Gkatzelis et al., 2018). Therefore, we cannot compare the fragmentation patterns of organic compounds from our instruments with those from other studies. However, it is consistent with other studies that the particulate oxidized organic compounds measured by the CHARON-PTR-ToF-MS in this study were mainly detected as the more abundant fragment ions after losing one H_2O molecule rather than as the parent ions.

3.2 Meteorological impacts on the variations of BVOCs

We firstly analyzed the variations in the mixing ratios of gas species as a function of wind direction (WD) with a bin of 10° (**Fig. 5**). According to the wind and geographical conditions around the sampling site (**Fig. 1b**), we divided the entire measurement period into four WD sectors including WD-forest (0-120°)), WD-cut (120-240°), WD-BPP (240-300°) and WD-village (300-330°). Within the sectors of WD-forest and WD-cut, the sampling site was influenced by an intact forest dominated by Norway spruce and a clear-cut area, respectively. In contrast, the sampling site was influenced by the winds coming from the BPP and the village residential areas within the sectors of WD-BPP and WD-village, respectively. We observed that the mixing ratios of CH_4 increased significantly in the WD-BPP along with the decrease of wind speeds and PBL heights and corresponding weaker dilution. In contrast, constantly low mixing ratios of CH_4 were observed in the WD-forest and WD-cut even when both wind speeds and PBL decreased significantly. The results indicate that the enhancement in CH_4 mixing ratios in the WD-BPP was mainly attributed to the BPP emissions. In addition, CH_4 mixing ratios remained higher for WD-village, which was likely associated with the anthropogenic emissions

from the village residential areas. We also observed a significant increase of monoterpene mixing ratios in the WD-BPP along with lower ambient temperature (~15 °C) and decreasing radiation. This suggests that the increase of monoterpene mixing ratios in the WD-BPP was due to BPP emissions rather than biogenic emissions. In contrast to CH_4, monoterpenes showed very low values in the WD-village, suggesting a minor contribution of anthropogenic emissions from the village residential areas to monoterpenes.

We also observed significant variations in the mixing ratios of isoprene, monoterpene and sesquiterpene in the WD-forest and WD-cut, likely associated with changes in meteorological conditions, biogenic emissions and/or chemical oxidation processes. Specifically, the mixing ratios of monoterpenes and sesquiterpenes increased in the WD-forest of 0-30° but isoprene showed no significant change. The meteorological condition in the WD-forest of 0-30° was characterized by low ambient temperature, low wind speed and shallow PBL during nighttime. Unlike isoprene, monoterpenes and sesquiterpenes can still be released from the Norway spruce in the dark (Van Meeningen et al., 2017). Monoterpenes and sesquiterpenes could accumulate during nighttime in the WD-forest of 0-30° as a result of low concentrations of atmospheric oxidants like O_3. Besides, we observed an increase of isoprene mixing ratios in the WD-forest of 60-120° which was coincided with the increases of wind speed, PBL, ambient temperature and radiation during daytime. In contrast, monoterpenes and sesquiterpenes showed low mixing ratios of in the WD-forest of 60-120°. It is expected that higher temperature and radiation enhanced biogenic emissions, resulting in the increase of isoprene mixing ratios. However, lower mixing ratios of monoterpenes and sesquiterpenes were likely attributed to the photochemical oxidation exceeding their biogenic emissions. The strong photochemical oxidation processes were characterized by higher radiation and O_3 mixing ratios in the WD-forest of 60-120°. In the WD-cut of 120-180°, we observed simultaneous increase of isoprene, monoterpenes and sesquiterpenes, which were associated with enhanced biogenic emissions induced by higher temperature. Conversely, simultaneous decrease of isoprene, monoterpenes and sesquiterpenes mixing ratios were observed in the WD-cut of 180-240° along with high ambient temperature. Note that the sampling site were more influenced by the distant Norway Spruce trees in the WD-cut of 120-180° compared to the WD-cut of 180-240° (**Fig. 1a**). In addition, the wind speeds were significantly higher in the WD-cut of 180-240°. Therefore, the decreases in isoprene, monoterpenes and sesquiterpenes mixing ratios in the WD-cut of 180-240° were attributed to the reduced biogenic emissions of fewer Norway spruce and the dilution effect caused by higher wind speeds. The dilution effect was supported by the lowest CO mixing ratios and BC mass concentrations observed in the WD-cut of 180-240°.

Based on the above WD analyses, we further investigated the diurnal variations of meteorological parameters as well as gas species in two major groups influenced by anthropogenic (WD-BPP and WD-village) and biogenic (WD-forest and WD-cut) emissions respectively (**Fig. 6**). In the anthropogenic-group, the diurnal variations of CH_4 mixing ratios showed higher values during nighttime, which were related to the BPP emissions, low wind speed and PBL height. However, a less pronounced diurnal variations of CH_4 mixing ratios were observed under the influence of biogenic-group. In the anthropogenic-group, the diurnal behavior of monoterpenes showed higher mixing ratios during nighttime but with large fluctuations over the whole day. These fluctuations with monoterpene spikes were related to the BPP emissions depending on the wind directions. As expected, isoprene showed higher concentrations during daytime in the biogenic-group, which is similar to the diurnal behavior of isoprene emission rate in previous observations in Norway-spruce-dominated forests (Bourtsoukidis et al., 2014; Juráň et al., 2017). However, in the biogenic-group, the diurnal variations of monoterpenes and sesquiterpenes showed very low mixing ratios during daytime due to the expanding PBL and strong photochemical consumption. The concentrations of monoterpenes and sesquiterpenes peaked at ~18:00 when the concentrations of atmospheric oxidants (OH radicals and O_3) and PBL heights decreased. Monoterpenes and sesquiterpenes showed low mixing ratios with <1 ppb and <0.01 ppb, respectively after 18:00 during nighttime in the biogenic-group. This is different with previous studies in the boreal forests where constantly higher mixing ratios of monoterpenes and sesquiterpenes but lower O_3 values (<20 ppb) were observed during nighttime compared to daytime (Hakola et al., 2012; Li et al., 2020). However, in our study, higher O_3 mixing ratios (~30 ppb) were observed during nighttime in the biogenic-group, which may have reduced the concentrations of monoterpenes and sesquiterpenes by nighttime oxidation. Note that the mixing ratios of monoterpenes and sesquiterpenes were low during daytime, but they increased slightly from 8:00-12:00 when the temperature and radiation increased. **Figure 7** shows the time series of isoprene, monoterpenes, sesquiterpenes and O_3 along with wind direction and ambient temperature during low-T and high-T episodes. During daytime of the high-T episode, we observed that the mixing ratios of isoprene, monoterpenes, sesquiterpenes all increased as the temperature increased when the sampling site was constantly influenced by the WD of ~100° from the intact forest. Meanwhile, higher radiation and constantly high mixing ratios of O_3 (40-60 ppb) were observed during daytime of the high-T episode. The photochemical O_3 production is supported by also by higher BVOC mixing ratios. However, the increasing biogenic emissions due to higher temperatures and solar radiation obviously exceeded the photochemical consumptions. Similarly, higher

mixing ratios of O_3 were observed during daytime of the low-T episode when the sampling site was also constantly influenced by the wind direction of ~100° (e.g., 11th of June). However, the mixing ratios of isoprene, monoterpenes, sesquiterpenes showed no increase. In **Fig. 7a**, we also found that very high mixing ratios of monoterpenes and sesquiterpenes during the low-T episode (e.g., 20:00-24:00, 10th of June) were associated with the changes of wind directions, which was in line with the WD analyses as discussed above. Besides, soil moisture showed no significant difference between the low-T and high-T episode (**Fig. 2**). We cannot demonstrate the impact of soil moisture on the variations of BVOC mixing ratios due to the observation period was short in this study.

3.3 Source apportionment of VOCs

In addition to meteorological impacts, the variations of VOC concentrations are influenced by different emission sources and chemical processes. We performed a PMF analysis of Vocus-PTR-ToF-MS-measured VOC data to identify and determine the impacts of different sources and oxidation processes. According to the factor profiles and temporal variations, we present a six-factor solution including one terpene-dominated factor, one factor related to BVOC oxidation during nighttime, one factor related to aromatic VOC oxidation and three factors related to daytime BVOC oxidation. **Figure 8** shows the factor profiles, time series and diurnal variations of six factors as well as their relative contribution to total VOCs (TVOCs) during the entire measurement campaign.

The first factor profile was dominated by the monoterpene parent ion ($C_{10}H_{17}^+$) and its fragment ion ($C_6H_9^+$) (Tani et al., 2003; Kari et al., 2018). Furthermore, this factor was characterized with higher fraction of monoterpenoids such as $C_{10}H_{17}O^+$ (camphor or monoterpene oxide) and $C_{10}H_{19}O^+$ (linalool or monoterpene water cluster) in high mass range (*m/z*140-230) (Li et al., 2020). These monoterpenoids can be emitted by leaves and flowers directly (Joó et al., 2010). Therefore, we define this factor as a terpene-dominated factor. As discussed before, the variations of monoterpene concentrations were influenced by the BPP emissions and biogenic emissions depending on the wind directions. In this study, PMF analysis could not separate the relative contribution of biogenic emissions and BPP emissions to monoterpenes directly. This is probably due to the source profile of BPP emissions dominated by the monoterpenes that is similar to that of biogenic emissions. Based on the WD analyses, this factor was expected to be mainly associated with the biogenic emissions when the winds were coming from the forest. In contrast, when the winds were coming from the BPP, this factor was significantly contributed by the BPP emissions.

The second factor profile was characterized with high fractions of $C_{10}H_{17}O^+$ (monoterpene oxide), $C_{10}H_{17}O_2^+$ and $C_{10}H_{15}O^+$ (pinonaldehyde and its fragment ion) in high mass range. These compounds were weakly-oxidized products of monoterpenes with oxygen atom number < 3 as found by previous studies (Li et al., 2021a; Li et al., 2020; Vermeuel et al., 2023). In addition, this factor was dominated by $C_3H_7O^+$ (acetone), which could be contributed by the primary emissions and the oxidation of VOCs from both biogenic and anthropogenic sources (Jacob et al., 2002). The diurnal pattern of second factor showed higher concentrations at nighttime. Therefore, we define this factor representing the secondary oxidation processes of BVOCs especially monoterpenes during nighttime (night-SecVOC). Li et al., (2021a) performed a binPMF analysis on Vocus-PTR-ToF-MS-measured VOC data at two European forest sites. They also resolved a factor representing weakly-oxidized products of monoterpenes with higher concentrations at night (Li et al., 2021a).

The third factor profile was characterized with higher fractions of $C_6H_7O^+$ (phenol), $C_6H_7O_2^+$ (catechol), and $C_7H_7O_2^+$ (benzoic acid) compared to other factors. Furthermore, this factor was dominated by $C_7H_9O_3^+$ (e.g., oxo-heptedienoic acid) and $C_8H_9O_3^+$ (e.g., vanillin) in high mass range. These OVOC species could originate from the oxidation of aromatic hydrocarbons (Hamilton et al., 2005; Zaytsev et al., 2019; Li et al., 2021b; Wu et al., 2014; Lannuque et al., 2023). As expected, good correlations were found for aromatic OVOC with catechol (r = 0.87 for $C_6H_7O_2^+$) and benzoic acid (r = 0.84 for $C_7H_7O_2^+$). In addition, this factor also correlated well (r = 0.77-0.87, **Fig. S10**) with $C_5H_5O_3^+$ (e.g., methylfurandione), $C_5H_5O_2^+$ (e.g., butenedial), $C_4H_5O_2^+$ (e.g., furfural), and $C_3H_5O_2^+$ (e.g., methylglyoxal). These compounds are likely ring-opening products of toluene oxidation as reported in previous studies (Zaytsev et al., 2019; Wu et al., 2014; Lannuque et al., 2023). Therefore, we identified this factor as a factor of aromatic OVOC representing the OVOCs formed from the oxidation of aromatic hydrocarbons. The diurnal variation of aromatic OVOC factor showed slightly higher concentrations during daytime, which can be related to an enhanced photochemical oxidation of aromatic hydrocarbons.

In this study, we also resolved three factors related to the oxidation of BVOCs during daytime denoted as day-SecVOC1, day-SecVOC2 and day-SecVOC3. The factor profile of day-SecVOC1 was characterized with high fractions of acetic acid ($C_2H_5O_2^+$) as well as isoprene and its oxidation products (e.g., $C_5H_9^+$, $C_4H_7O_{1\text{-}4}^+$ and $C_5H_9O_{2\text{-}4}^+$). This factor was also dominated by stronger oxidized products of monoterpenes with oxygen atom numbers >3 (e.g., $C_{10}H_{17}O_{4\text{-}5}^+$) compared to other factors in the higher mass range. The diurnal variations of day-

SecVOC1 factor showed high concentrations during daytime. Therefore, the day-SecVOC1 factor can be mainly attributed to the photochemical oxidation of isoprene and monoterpenes during daytime. Li et al., (2021a) resolved one factor representing isoprene and its oxidation products and another factor representing stronger oxidized products of monoterpenes from the binPMF analysis for a low-mass (*mz*50-200) and a high-mass range (*mz*201-320), respectively, for two European forest sites. They found that these two factors had a similar diurnal pattern with high daytime concentrations. In our study, we performed the PMF analysis for the full mass range (m/z40-220) of the major VOC ions and resolved the day-SecVOC1 factor containing high fractions of oxidized products of isoprene and monoterpenes. This suggests that isoprene oxidation products and higher oxidized products of monoterpenes were mainly related to the daytime oxidation processes. The factor profiles of both day-SecVOC2 and day-SecVOC3 were characterized with high fractions of acetone ($C_3H_7O^+$) and acetic acid ($C_2H_5O_2^+$). Acetone and acetic acid could be contributed by biogenic and anthropogenic secondary sources (Khare et al., 1999; Jacob et al., 2002). The factor profile of day-SecVOC2 also had high fractions of $C_2H_7O_3^+$ (acetic acid water cluster), $C_3H_7O_2^+$ (propionic acid), $C_4H_9O_2^+$ (butyric acid) and $C_3H_9O_2^+$ (e.g., propylene glycol). These gaseous organic acids could be formed from the oxidation of BVOCs like monoterpenes (Friedman and Farmer, 2018). In addition, the factor profile of day-SecVOC3 showed higher fractions of $C_4H_7O_4^+$ (e.g., succinic acid) compared to other factors. The time series of day-SecVOC3 showed the highest correlations with $C_2H_7O_3^+$ (acetic acid water cluster, r = 0.79), $C_2H_5O_2^+$ (acetic acid, r = 0.63) and $C_3H_9O_3^+$ (propionic acid water cluster) compared to other factors. The time series of day-SecVOC3 factor also showed strong correlations with $C_4H_6O^+$ (r = 0.90, **Fig. S10**) and $C_2H_5O_3^+$ (r = 0.89), which can be assigned as the isoprene oxidation product as deprotonated $C_4H_7O^+$ (MVK+MACR) and glycolic acid, respectively. In addition, O_3 was only weakly correlated with day-SecVOC2 (r = 0.27), but much better correlated with day-SecVOC3 (r = 0.57). Moreover, a better correlation was found between O_3 and the sum of these two factors (r = 0.70). The diurnal variations of both factors showed higher concentrations during daytime. Based on these results, we identified day-SecVOC2 and day-SecVOC3 as representing low-molecular weight oxygenated organic compounds produced from the daytime photooxidation of BVOCs.

As shown in **Fig. 8**, the mixing ratios of TVOCs measured by the Vocus-PTR-ToF-MS for the PMF analysis was 9.0 ± 4.4 ppb during the entire campaign. The mixing ratios of TVOCs was dominated by the daytime BVOC oxidation with day-SecVOC1 (8% ± 5%), day-SecVOC2 (27% ± 20%), day-SecVOC3 (18% ± 21%). This indicates substantial contributions of

oxygenated species to TVOCs during the entire campaign. Based on the WD analysis, we further compared the relative contributions of VOC factors to TVOCs for the groups influenced by the biogenic and anthropogenic emissions, respectively. The average concentration of TVOCs in the biogenic-group (9.7 ± 4.7 ppb) were slightly higher than that in the anthropogenic-group (7.1 ± 3.6 ppb). The contribution of day-SecVOC2 to TVOCs was comparable with 25% ± 21% and 32% ± 18% for the biogenic- and anthropogenic-group, respectively. However, the contribution of day-SecVOC3 to TVOCs in the biogenic-group (26% ± 25%) was higher than that in the anthropogenic-group (13% ± 15%). We observed significantly elevated mixing ratios of isoprene (**Fig. 3c**) and day-SecVOC3 during the high-T episode (**Fig. 8**). As mentioned before, the sampling site was mainly influenced by the winds coming from the forest during high-T episode along with higher mixing ratios of O_3. Therefore, higher contribution of day-SecVOC3 in the biogenic-group was attributed to the strong oxidation of BVOCs especially of isoprene. The contribution of terpene-dominated factor to TVOCs was higher in the anthropogenic-group (18% ± 16%) compared to that in the biogenic-group (11% ± 15%). This is consistent with the WD analyses that higher monoterpene mixing ratios were related to the BPP emissions. In addition, the contributions of night-SecVOC and day-SecVOC1 factors to TVOCs concentrations were slightly higher in the anthropogenic-group, which were related to high abundances of monoterpenes. Furthermore, gas-to-particle partitioning processes could also influence the variations of BVOC oxidation products and thus night-SecVOC and day-SecVOC1 factors.

3.4 Variations of BVOC oxidation products in gas- and particle phases

Figure 9 shows the diurnal variations of concentrations of organic molecules ($C_5H_9O_{1\text{-}4}^+$, $C_4H_7O_{1\text{-}4}^+$, $C_{10}H_{17}O_{1\text{-}5}^+$ and $C_{10}H_{15}O_{1\text{-}5}^+$) in the gas phase measured by the Vocus-PTR-ToF-MS and particle phase compounds measured by the CHARON-PTR-ToF-MS during 22nd-30th of June. These organic molecules are important components of night-SecVOC and day-SecVOC1 factors resolved by the PMF analysis, and they are identified as the oxidation products from isoprene and monoterpenes based on previous field observations and simulation chamber experiments (Gkatzelis et al., 2018; Li et al., 2020). For example, gaseous $C_4H_7O^+$ can be the sum of methyl vinyl ketone (MVK) and methacrolein (MACR), which are major products of the isoprene oxidation (Wennberg et al., 2018). $C_{10}H_{17}O_3^+$ can be attributed to *cis*-pinonic acid formed from the oxidation of monoterpenes (e.g., α-pinene). Again, the fragmentation of high-molecular weight oxidized organic compounds measured by the PTR-ToF-MS instruments could produce the fragment ions via the loss of neutral water, carbonyl, or carboxyl

groups (-H_2O, -CO and -CO_2). The diurnal variations of all isoprene oxidation products ($C_5H_9O_{1-4}^+$ and $C_4H_7O_{1-4}^+$) in both gas and particle phases showed higher concentrations from morning (6:00-8:00) to afternoon (12:00-16:00) as well as isoprene itself. These results indicate that higher temperatures and intensive sunlight not only favor the isoprene emissions but also enhance photochemical oxidation of isoprene. Besides, we found that the concentrations of particulate $C_4H_7O_{1-2}^+$ showed increased values from early nighttime (18:00-20:00) to midnight (0:00-2:00 of the next day). As mentioned before, the fragmentation of *cis*-pinonic acid in the CHARON-PTR-ToF-MS can produce the fragment ions $C_4H_7O^+$, $C_6H_{11}O_2$+ and $C_{10}H_{15}O_2^+$ (Gkatzelis et al., 2018; Peng et al., 2023; Muller et al., 2017; Leglise et al., 2019). Furthermore, we observed a similar diurnal pattern of $C_4H_7O^+$and $C_{10}H_{15}O_2^+$ in the particle phase, suggesting that the nighttime increase of particulate $C_4H_7O^+$ was likely contributed by the fragmentation of *cis*-pinonic acid. Due to instrumental limitation, it is difficult to assign each ion detected by the PTR-ToF-MS to either parent ion or fragment ion of one organic compound in the ambient particles.

The diurnal variations of weakly-oxidized products of monoterpenes like $C_{10}H_{17}O_{1-2}^+$ and $C_{10}H_{15}O_{1-2}^+$ in both gas and particle phases showed elevated concentrations during nighttime. In contrast, the more-oxidized products of monoterpenes ($C_{10}H_{17}O_{4-5}^+$ and $C_{10}H_{15}O_{4-5}^+$) showed higher concentrations in gas and particle phases during daytime. The higher atmospheric oxidation capacity during daytime compared to nighttime leads to the formation of more-oxidized products. In addition, $C_{10}H_{17}O_3^+$ (*cis*-pinonic acid) and its fragment ion ($C_{10}H_{15}O_2^+$) in the gas phase showed less pronounced diurnal patterns. The particulate $C_{10}H_{17}O_3^+$ also showed a less pronounced diurnal behavior, while the particulate $C_{10}H_{15}O_2^+$ showed increased concentrations during nighttime. This is in agreement with previous findings that most of the particulate compounds detected by the CHARON-PTR-ToF-MS were not detected as the parent ion but as the fragment ion with one H_2O molecule lost (Gkatzelis et al., 2018). In this study, $C_{14}H_{23}O_2^+$, $C_{15}H_{23}O^+$, $C_{15}H_{25}O_2^+$ were measured by the PTR instruments, which can be considered as the sesquiterpene oxidation products based on previous field and simulation chamber studies. Here $C_{14}H_{23}O_2^+$ was detected only in the gas phase by the Vocus-PTR-ToF-MS, while $C_{15}H_{23}O_2^+$ and $C_{15}H_{25}O_2^+$ were detected only in the particle phase by the CHARON-PTR-ToF-MS. The concentrations of sesquiterpene oxidation products in both gas (<0.5 ppt) and particle phases (<5 ng m^{-3}) were relatively low probably due to correspondingly low concentrations of sesquiterpenes in this study. The diurnal pattern of gaseous $C_{14}H_{23}O_2^+$ showed two peaks in the morning and early evening (**Fig. S11**), which was similar to those of weakly-oxidized products of sesquiterpenes (e.g., $C_{14}H_{22}O_{1-3}$ and $C_{15}H_{24}O_{1-3}$) observed at the Landes

642 forest in France (Li et al., 2020). The diurnal variations of particulate $C_{15}H_{23}O_2^+$ and $C_{15}H_{25}O_2^+$
643 showed slightly higher values during nighttime.

644 Furthermore, we calculated the variations of OA/ΔCO, which are the total OA
645 concentrations measured by the CHARON-PTR-ToF-MS normalized over ΔCO (subtracted by
646 the background CO concentration) during 22nd-30th of June (**Fig. 10**). CO is relatively long-
647 lived, normalizing the observed OA mass concentrations to the background-corrected CO helps
648 to minimize the impacts of boundary layer dynamics (De Gouw and Jimenez, 2009). An
649 increase of OA/ΔCO was observed during nighttime of the high-T episode, which could be
650 related to the gas-to-particle partitioning of BVOC oxidation products. Based on the two PTR
651 measurements, we calculated the particulate fraction of representative monoterpene oxidation
652 products (i.e., $C_{10}H_{17}O_{1\text{-}3}^+$ and $C_{10}H_{15}O_{1\text{-}5}^+$) to estimate their gas gas-to-particle partitioning
653 processes. The two PTR instruments used in this study may have different sensitivities or
654 fragmentation for different oxygenated organic compounds. For example, the concentrations of
655 monoterpene oxidation products such as $C_9H_{15}O^+$, $C_{10}H_{15}O_{1\text{-}2}^+$ and $C_{10}H_{17}^+$ measured by the
656 Vocus-PTR-ToF-MS were ~2-3 times higher than those measured by the CHARON-PTR-ToF-
657 MS (**Fig. S13b**). Although we cannot precisely calculate the F_p values for each OA molecule
658 due to instrumental limitations, the variations of calculated F_p values can still be used as an
659 indicator for estimating the gas-to-particle portioning processes. As shown in **Fig. 10**, weakly-
660 oxidized molecules of monoterpenes ($C_{10}H_{17}O_{1\text{-}2}^+$ and $C_{10}H_{15}O_{1\text{-}3}^+$) had lower F_p values
661 compared to more-oxidized molecules of monoterpenes ($C_{10}H_{17}O_3^+$ and $C_{10}H_{15}O_{4\text{-}5}^+$). This is
662 expected because more-oxidized products of monoterpenes generally have lower volatility
663 compared to weakly-oxidized ones. Interestingly, the F_p values of weakly-oxidized molecules
664 of monoterpenes showed similar temporal trends as the relative humidity. Especially for the
665 high-T episode, the F_p values of weakly-oxidized molecules of monoterpenes ($C_{10}H_{15}O_{1\text{-}3}^+$)
666 showed positive correlations (r = 0.65-0.71) with RH. This indicates that increasing RH can
667 enhance the particle fraction of weakly-oxidized molecules of monoterpenes and thus increase
668 SOA mass. As validated in Section 3.3, these weakly-oxidized molecules of monoterpenes are
669 formed by oxidation of monoterpenes emitted from trees during the high-T episode rather than
670 from BPP emissions. It is reasonable to assume that these monoterpenes are mainly α-pinene
671 and β-pinene because our sampling site was in a forest dominated by Norway spruce known to
672 emit mainly pinenes (Christensen et al., 2000; Hakola et al., 2017). Previously, Tillmann et al.,
673 (2010) found that the SOA yields from the ozonolysis of α-pinene were higher at humid
674 conditions than at dry conditions. More recently, Surdu et al., (2023) studied the effect of RH
675 on the partitioning of oxidized organic molecules formed from α-pinene oxidation at the CERN

CLOUD chamber. They observed that the particle-phase concentrations of semi-volatile organic molecules ($C_{10}H_{16}O_{2-3}$) from α-pinene oxidation significantly increases by factors of 2-4 with increasing RH, thus leading to a substantial increase of SOA mass (Surdu et al., 2023). Similarly, Luo et al., (2024) reported that increasing RH from 3% to 84% increase the abundance of less oxidized products (e.g., $C_{10}H_{16}O_{2-6}$) from α-pinene ozonolysis. In our study, during the high-T episode, we observed the F_p values for $C_{10}H_{15}O^+$, $C_{10}H_{15}O_2^+$ and $C_{10}H_{15}O_3^+$ increased by ~2%, ~6% and ~20% respectively when RH was increased from 30-40% to 60-80%. Besides, the ambient temperature was anticorrelated with RH in this study. Thus, lower temperatures may further additionally favor the gas-to-particle partitioning of semi-volatile organic molecules from monoterpene oxidation.

4 Conclusions

In this study, we investigated the characteristics of VOCs and OA particles simultaneously measured by a CHARON-PTR-ToF-MS and a Vocus-PTR-ToF-MS at a Norway-spruce-dominated forest stressed by bark beetles and droughts close to a BPP in western Germany during June 2020. The average mass concentration of OA particles detected by the CHARON-PTR-ToF-MS was 0.8 ± 0.5 μg m^{-3}. The chemical composition of OA ions ranged between C_2 and C_{10} with oxygen atom numbers of 0-5, which were mainly attributed to the semi-volatile organic compounds formed from monoterpene oxidation. The average mixing ratios of isoprene and monoterpenes were higher than the values previously measured in both German temperate forests and boreal forests during summertime (Mermet et al., 2021; Li et al., 2021a; Hellén et al., 2018; Bourtsoukidis et al., 2014) which may be due to stressed trees with long lasting droughts and bark beetle infestation and differences in the meteorological conditions. Based on the WD analyses, BVOC data were categorized into two groups to distinguish the impacts of biogenic emissions from an intact forest and a clear cut (biogenic-group) and anthropogenic emissions from a BPP and a village (anthropogenic-group). The mixing ratios of CH_4 and monoterpenes showed significantly higher values in the anthropogenic-group. This was expected for CH_4, and it is also known that BPP can release high concentrations of monoterpenes during biowaste storage and fermentation processes (Salazar Gómez et al., 2016; Papurello et al., 2012). In the biogenic-group, the variations in mixing ratios of isoprene, monoterpenes and sesquiterpenes were driven by the interplay between meteorological conditions, biogenic emissions and subsequent chemical oxidation processes. Based on the PMF analysis of VOCs measured by the Vocus-PTR-ToF-MS, six factors were resolved, representing the major sources and/or products of chemical transformation processes. During

the entire measurement period, TVOCs were largely composed of oxygenated organic compounds formed from the photochemical oxidation of BVOCs during daytime. However, monoterpenes and their weakly-oxidized products (e.g., $C_{10}H_{15}O_{1\text{-}3}^{+}$ and $C_{10}H_{17}O_{1\text{-}2}^{+}$) dominated the TVOCs during nighttime. These weakly-oxidized monoterpene products in the particle phase also showed higher mixing ratios during nighttime. In contrast, more-oxidized monoterpene products (e.g., $C_{10}H_{17}O_{4\text{-}5}^{+}$ and $C_{10}H_{15}O_{4\text{-}5}^{+}$) in both gas and particle phases were more abundant during daytime. By combining the gas and particle data measured by the CHARON-PTR-ToF-MS and the Vocus-PTR-ToF-MS, we found that increasing RH and decreasing temperature led to an increase in the particulate fraction of weakly-oxidized monoterpene products, consistent with the findings from recent simulation chamber studies (Surdu et al., 2023; Luo et al., 2024). Overall, this study demonstrates that the variations of BVOCs are influenced not only by meteorology and biogenic emissions but also by local anthropogenic emissions (e.g., from a BPP), and subsequent chemical transformation processes in a typical stressed European coniferous forest. The impact of soil moisture, tree species composition and tree health conditions on the variations of BVOC concentrations could not be fully addressed due to the relative short observation period. Future long-term field measurements including seasonality and detailed tree characterization are necessary to assess the impacts of droughts and bark beetle outbreaks on BVOC emissions and subsequent formation of SOA.

Data availability

Data shown in the paper are available via the KIT data repository KITopen (link will be added).

Author contributions

JS, HS and RT conducted the field measurements. JS and GG carried out the data analysis of CHARON-PTR-ToF-MS and Vocus-PTR-ToF-MS respectively. NB and TL gave general comments for this paper. JS drafted the manuscript with contributions from all co-authors.

Competing interest

At least one of the (co-)authors is a member of the editorial board of Atmospheric Chemistry and Physics.

Acknowledgement

This work was supported by the Modular Observation Solutions for Earth Systems (MOSES) project, a novel observing system of the Helmholtz Association. Financial support by China

Scholarship Council (CSC) for JS is gratefully acknowledged. We gratefully acknowledged the TERENO (Terrestrial Environmental Observatories) funded by the Helmholtz-Gemeinschaft. The authors acknowledged Heye Bogena for providing daily soil moisture data as well as Christian Wesolek, Sergej Wedel, and Doreen Niether for their technical support in field measurement deployment.

References

Atkinson, R.: Atmospheric chemistry of VOCs and NOx, Atmos. Environ., 34, 2063-2101, https://doi.org/10.1016/S1352-2310(99)00460-4, 2000.

Bakkaloglu, S., Lowry, D., Fisher, R. E., France, J. L., Brunner, D., Chen, H., and Nisbet, E. G.: Quantification of methane emissions from UK biogas plants, Waste Manage, 124, 82-93, https://doi.org/10.1016/j.wasman.2021.01.011, 2021.

Bogena, H. R., Huisman, J. A., Güntner, A., Hübner, C., Kusche, J., Jonard, F., Vey, S., and Vereecken, H.: Emerging methods for noninvasive sensing of soil moisture dynamics from field to catchment scale: a review, WIREs Water, 2, 635-647, https://doi.org/10.1002/wat2.1097, 2015.

Bonn, B., Magh, R. K., Rombach, J., and Kreuzwieser, J.: Biogenic isoprenoid emissions under drought stress: different responses for isoprene and terpenes, Biogeosciences, 16, 4627-4645, 10.5194/bg-16-4627-2019, 2019.

Bourtsoukidis, E., Williams, J., Kesselmeier, J., Jacobi, S., and Bonn, B.: From emissions to ambient mixing ratios: online seasonal field measurements of volatile organic compounds over a Norway spruce-dominated forest in central Germany, Atmos. Chem. Phys., 14, 6495-6510, 10.5194/acp-14-6495-2014, 2014.

Bourtsoukidis, E., Pozzer, A., Williams, J., Makowski, D., Peñuelas, J., Matthaios, V. N., Lazoglou, G., Yañez-Serrano, A. M., Lelieveld, J., Ciais, P., Vrekoussis, M., Daskalakis, N., and Sciare, J.: High temperature sensitivity of monoterpene emissions from global vegetation, Communications Earth & Environment, 5, 23, 10.1038/s43247-023-01175-9, 2024.

Brémond, U., Bertrandias, A., Steyer, J.-P., Bernet, N., and Carrere, H.: A vision of European biogas sector development towards 2030: Trends and challenges, J. Clean. Prod., 287, 125065, https://doi.org/10.1016/j.jclepro.2020.125065, 2021.

Byron, J., Kreuzwieser, J., Purser, G., van Haren, J., Ladd, S. N., Meredith, L. K., Werner, C., and Williams, J.: Chiral monoterpenes reveal forest emission mechanisms and drought responses, Nature, 609, 307-312, 10.1038/s41586-022-05020-5, 2022.

Christensen, C. S., Hummelshøj, P., Jensen, N. O., Larsen, B., Lohse, C., Pilegaard, K., and Skov, H.: Determination of the terpene flux from orange species and Norway spruce by relaxed eddy accumulation, Atmos. Environ., 34, 3057-3067, https://doi.org/10.1016/S1352-2310(99)00502-6, 2000.

De Gouw, J. and Jimenez, J. L.: Organic Aerosols in the Earth's Atmosphere, Environ. Sci. Technol., 43, 7614-7618, 10.1021/es9006004, 2009.

Desservettaz, M., Pikridas, M., Stavroulas, I., Bougiatioti, A., Liakakou, E., Hatzianastassiou, N., Sciare, J., Mihalopoulos, N., and Bourtsoukidis, E.: Emission of volatile organic compounds from residential biomass burning and their rapid chemical transformations, Science of The Total Environment, 903, 166592, https://doi.org/10.1016/j.scitotenv.2023.166592, 2023.

Eichler, P., Muller, M., D'Anna, B., and Wisthaler, A.: A novel inlet system for online chemical analysis of semi-volatile submicron particulate matter, Atmos. Meas. Tech., 8, 1353-1360, 10.5194/amt-8-1353-2015, 2015.

Faiola, C. and Taipale, D.: Impact of insect herbivory on plant stress volatile emissions from trees: A synthesis of quantitative measurements and recommendations for future research, Atmospheric Environment: X, 5, 100060, https://doi.org/10.1016/j.aeaoa.2019.100060, 2020.

Friedman, B. and Farmer, D. K.: SOA and gas phase organic acid yields from the sequential photooxidation of seven monoterpenes, Atmos. Environ., 187, 335-345, https://doi.org/10.1016/j.atmosenv.2018.06.003, 2018.

Ghimire, R. P., Kivimäenpää, M., Blomqvist, M., Holopainen, T., Lyytikäinen-Saarenmaa, P., and Holopainen, J. K.: Effect of bark beetle (Ips typographus L.) attack on bark VOC emissions of Norway spruce (Picea abies Karst.) trees, Atmospheric Environment, 126, 145-152, https://doi.org/10.1016/j.atmosenv.2015.11.049, 2016.

Gkatzelis, G. I., Coggon, M. M., McDonald, B. C., Peischl, J., Gilman, J. B., Aikin, K. C., Robinson, M. A., Canonaco, F., Prevot, A. S. H., Trainer, M., and Warneke, C.: Observations Confirm that Volatile Chemical Products Are a Major Source of Petrochemical Emissions in U.S. Cities, Environ. Sci. Technol., 55, 4332-4343, 10.1021/acs.est.0c05471, 2021.

Gkatzelis, G. I., Tillmann, R., Hohaus, T., Müller, M., Eichler, P., Xu, K. M., Schlag, P., Schmitt, S. H., Wegener, R., Kaminski, M., Holzinger, R., Wisthaler, A., and Kiendler-Scharr, A.: Comparison of

three aerosol chemical characterization techniques utilizing PTR-ToF-MS: a study on freshly formed and aged biogenic SOA, Atmos. Meas. Tech., 11, 1481-1500, 10.5194/amt-11-1481-2018, 2018.

Guenther, A. B., Jiang, X., Heald, C. L., Sakulyanontvittaya, T., Duhl, T., Emmons, L. K., and Wang, X.: The Model of Emissions of Gases and Aerosols from Nature version 2.1 (MEGAN2.1): an extended and updated framework for modeling biogenic emissions, Geosci. Model Dev., 5, 1471-1492, 10.5194/gmd-5-1471-2012, 2012.

Hakola, H., Hellén, H., Hemmilä, M., Rinne, J., and Kulmala, M.: In situ measurements of volatile organic compounds in a boreal forest, Atmos. Chem. Phys., 12, 11665-11678, 10.5194/acp-12-11665-2012, 2012.

Hakola, H., Tarvainen, V., Praplan, A. P., Jaars, K., Hemmilä, M., Kulmala, M., Bäck, J., and Hellén, H.: Terpenoid and carbonyl emissions from Norway spruce in Finland during the growing season, Atmos. Chem. Phys., 17, 3357-3370, 10.5194/acp-17-3357-2017, 2017.

Hallquist, M., Wenger, J. C., Baltensperger, U., Rudich, Y., Simpson, D., Claeys, M., Dommen, J., Donahue, N. M., George, C., Goldstein, A. H., Hamilton, J. F., Herrmann, H., Hoffmann, T., Iinuma, Y., Jang, M., Jenkin, M. E., Jimenez, J. L., Kiendler-Scharr, A., Maenhaut, W., McFiggans, G., Mentel, T. F., Monod, A., Prévôt, A. S. H., Seinfeld, J. H., Surratt, J. D., Szmigielski, R., and Wildt, J.: The formation, properties and impact of secondary organic aerosol: current and emerging issues, Atmos. Chem. Phys., 9, 5155-5236, 10.5194/acp-9-5155-2009, 2009.

Hamilton, J. F., Webb, P. J., Lewis, A. C., and Reviejo, M. M.: Quantifying small molecules in secondary organic aerosol formed during the photo-oxidation of toluene with hydroxyl radicals, Atmospheric Environment, 39, 7263-7275, https://doi.org/10.1016/j.atmosenv.2005.09.006, 2005.

Hellén, H., Praplan, A. P., Tykkä, T., Ylivinkka, I., Vakkari, V., Bäck, J., Petäjä, T., Kulmala, M., and Hakola, H.: Long-term measurements of volatile organic compounds highlight the importance of sesquiterpenes for the atmospheric chemistry of a boreal forest, Atmos. Chem. Phys., 18, 13839-13863, 10.5194/acp-18-13839-2018, 2018.

Hersbach, H., Bell, B., Berrisford, P., Hirahara, S., Horányi, A., Muñoz-Sabater, J., Nicolas, J., Peubey, C., Radu, R., Schepers, D., Simmons, A., Soci, C., Abdalla, S., Abellan, X., Balsamo, G., Bechtold, P., Biavati, G., Bidlot, J., Bonavita, M., De Chiara, G., Dahlgren, P., Dee, D., Diamantakis, M., Dragani, R., Flemming, J., Forbes, R., Fuentes, M., Geer, A., Haimberger, L., Healy, S., Hogan, R. J., Hólm, E., Janisková, M., Keeley, S., Laloyaux, P., Lopez, P., Lupu, C., Radnoti, G., de Rosnay, P., Rozum, I., Vamborg, F., Villaume, S., and Thépaut, J.-N.: The ERA5 global reanalysis, Quarterly Journal of the Royal Meteorological Society, 146, 1999-2049, https://doi.org/10.1002/qj.3803, 2020.

Huang, W., Saathoff, H., Shen, X., Ramisetty, R., Leisner, T., and Mohr, C.: Chemical Characterization of Highly Functionalized Organonitrates Contributing to Night-Time Organic Aerosol Mass Loadings and Particle Growth, Environ. Sci. Technol., 53, 1165-1174, 10.1021/acs.est.8b05826, 2019.

Huang, W., Li, H., Sarnela, N., Heikkinen, L., Tham, Y. J., Mikkilä, J., Thomas, S. J., Donahue, N. M., Kulmala, M., and Bianchi, F.: Measurement report: Molecular composition and volatility of gaseous organic compounds in a boreal forest – from volatile organic compounds to highly oxygenated organic molecules, Atmos. Chem. Phys., 21, 8961-8977, 10.5194/acp-21-8961-2021, 2021.

Isaacman-VanWertz, G., Yee, L. D., Kreisberg, N. M., Wernis, R., Moss, J. A., Hering, S. V., de Sá, S. S., Martin, S. T., Alexander, M. L., Palm, B. B., Hu, W., Campuzano-Jost, P., Day, D. A., Jimenez, J. L., Riva, M., Surratt, J. D., Viegas, J., Manzi, A., Edgerton, E., Baumann, K., Souza, R., Artaxo, P., and Goldstein, A. H.: Ambient Gas-Particle Partitioning of Tracers for Biogenic Oxidation, Environ. Sci. Tech., 50, 9952-9962, 10.1021/acs.est.6b01674, 2016.

Jaakkola, E., Gärtner, A., Jönsson, A. M., Ljung, K., Olsson, P. O., and Holst, T.: Spruce bark beetles (Ips typographus) cause up to 700 times higher bark BVOC emission rates compared to healthy Norway spruce (Picea abies), Biogeosciences, 20, 803-826, 10.5194/bg-20-803-2023, 2023.

Jacob, D. J., Field, B. D., Jin, E. M., Bey, I., Li, Q., Logan, J. A., Yantosca, R. M., and Singh, H. B.: Atmospheric budget of acetone, J. Geophys. Res. Atmos., 107, ACH 5-1-ACH 5-17, https://doi.org/10.1029/2001JD000694, 2002.

Jain, V., Tripathi, N., Tripathi, S. N., Gupta, M., Sahu, L. K., Murari, V., Gaddamidi, S., Shukla, A. K., and Prevot, A. S. H.: Real-time measurements of non-methane volatile organic compounds in the

857 central Indo-Gangetic basin, Lucknow, India: source characterisation and their role in O3 and
858 secondary organic aerosol formation, Atmos. Chem. Phys., 23, 3383-3408, 10.5194/acp-23-3383-
859 2023, 2023.
860 Joó, É., Van Langenhove, H., Šimpraga, M., Steppe, K., Amelynck, C., Schoon, N., Müller, J. F., and
861 Dewulf, J.: Variation in biogenic volatile organic compound emission pattern of Fagus sylvatica L.
862 due to aphid infection, Atmos. Environ., 44, 227-234,
863 https://doi.org/10.1016/j.atmosenv.2009.10.007, 2010.
864 Jordan, A., Haidacher, S., Hanel, G., Hartungen, E., Mark, L., Seehauser, H., Schottkowsky, R., Sulzer,
865 P., and Mark, T. D.: A high resolution and high sensitivity proton-transfer-reaction time-of-flight
866 mass spectrometer (PTR-TOF-MS), International Journal of Mass Spectrometry, 286, 122-128,
867 10.1016/j.ijms.2009.07.005, 2009.
868 Juráň, S., Pallozzi, E., Guidolotti, G., Fares, S., Šigut, L., Calfapietra, C., Alivernini, A., Savi, F.,
869 Večeřová, K., Křůmal, K., Večeřa, Z., and Urban, O.: Fluxes of biogenic volatile organic compounds
870 above temperate Norway spruce forest of the Czech Republic, Agricultural and Forest Meteorology,
871 232, 500-513, https://doi.org/10.1016/j.agrformet.2016.10.005, 2017.
872 Kari, E., Miettinen, P., Yli-Pirilä, P., Virtanen, A., and Faiola, C. L.: PTR-ToF-MS product ion
873 distributions and humidity-dependence of biogenic volatile organic compounds, International
874 Journal of Mass Spectrometry, 430, 87-97, https://doi.org/10.1016/j.ijms.2018.05.003, 2018.
875 Kari, E., Faiola, C. L., Isokääntä, S., Miettinen, P., Yli-Pirilä, P., Buchholz, A., Kivimäenpää, M.,
876 Mikkonen, S., Holopainen, J. K., and Virtanen, A.: Time-resolved characterization of biotic stress
877 emissions from Scots pines being fed upon by pine weevil by means of PTR-ToF-MS, 2019.
878 Khare, P., Kumar, N., Kumari, K. M., and Srivastava, S. S.: Atmospheric formic and acetic acids: An
879 overview, Reviews of Geophysics, 37, 227-248, https://doi.org/10.1029/1998RG900005, 1999.
880 Kleist, E., Mentel, T. F., Andres, S., Bohne, A., Folkers, A., Kiendler-Scharr, A., Rudich, Y., Springer,
881 M., Tillmann, R., and Wildt, J.: Irreversible impacts of heat on the emissions of monoterpenes,
882 sesquiterpenes, phenolic BVOC and green leaf volatiles from several tree species, Biogeosciences,
883 9, 5111-5123, 10.5194/bg-9-5111-2012, 2012.
884 Krechmer, J., Lopez-Hilfiker, F., Koss, A., Hutterli, M., Stoermer, C., Deming, B., Kimmel, J.,
885 Warneke, C., Holzinger, R., Jayne, J., Worsnop, D., Fuhrer, K., Gonin, M., and de Gouw, J.:
886 Evaluation of a New Reagent-Ion Source and Focusing Ion–Molecule Reactor for Use in Proton-
887 Transfer-Reaction Mass Spectrometry, Analytical Chemistry, 90, 12011-12018,
888 10.1021/acs.analchem.8b02641, 2018.
889 Lannuque, V., D'Anna, B., Kostenidou, E., Couvidat, F., Martinez-Valiente, A., Eichler, P., Wisthaler,
890 A., Müller, M., Temime-Roussel, B., Valorso, R., and Sartelet, K.: Gas–particle partitioning of
891 toluene oxidation products: an experimental and modeling study, Atmos. Chem. Phys., 23, 15537-
892 15560, 10.5194/acp-23-15537-2023, 2023.
893 Lee, B. H., Lopez-Hilfiker, F. D., D'Ambro, E. L., Zhou, P., Boy, M., Petäjä, T., Hao, L., Virtanen, A.,
894 and Thornton, J. A.: Semi-volatile and highly oxygenated gaseous and particulate organic
895 compounds observed above a boreal forest canopy, Atmos. Chem. Phys., 18, 11547-11562,
896 10.5194/acp-18-11547-2018, 2018.
897 Leglise, J., Müller, M., Piel, F., Otto, T., and Wisthaler, A.: Bulk Organic Aerosol Analysis by Proton-
898 Transfer-Reaction Mass Spectrometry: An Improved Methodology for the Determination of Total
899 Organic Mass, O:C and H:C Elemental Ratios, and the Average Molecular Formula, Anal. Chem.,
900 91, 12619-12624, 10.1021/acs.analchem.9b02949, 2019.
901 Li, H., Riva, M., Rantala, P., Heikkinen, L., Daellenbach, K., Krechmer, J. E., Flaud, P. M., Worsnop,
902 D., Kulmala, M., Villenave, E., Perraudin, E., Ehn, M., and Bianchi, F.: Terpenes and their oxidation
903 products in the French Landes forest: insights from Vocus PTR-TOF measurements, Atmos. Chem.
904 Phys., 20, 1941-1959, 10.5194/acp-20-1941-2020, 2020.
905 Li, H., Canagaratna, M. R., Riva, M., Rantala, P., Zhang, Y., Thomas, S., Heikkinen, L., Flaud, P. M.,
906 Villenave, E., Perraudin, E., Worsnop, D., Kulmala, M., Ehn, M., and Bianchi, F.: Atmospheric
907 organic vapors in two European pine forests measured by a Vocus PTR-TOF: insights into
908 monoterpene and sesquiterpene oxidation processes, Atmos. Chem. Phys., 21, 4123-4147,
909 10.5194/acp-21-4123-2021, 2021a.
910 Li, X. B., Yuan, B., Wang, S., Wang, C., Lan, J., Liu, Z., Song, Y., He, X., Huangfu, Y., Pei, C., Cheng,
911 P., Yang, S., Qi, J., Wu, C., Huang, S., You, Y., Chang, M., Zheng, H., Yang, W., Wang, X., and

912 Shao, M.: Variations and sources of volatile organic compounds (VOCs) in urban region: insights
913 from measurements on a tall tower, Atmos. Chem. Phys., 22, 10567-10587, 10.5194/acp-22-10567-
914 2022, 2022.
915 Li, Y., Zhao, J., Wang, Y., Seinfeld, J. H., and Zhang, R.: Multigeneration Production of Secondary
916 Organic Aerosol from Toluene Photooxidation, Environ. Sci. Technol., 55, 8592-8603,
917 10.1021/acs.est.1c02026, 2021b.
918 Luo, H., Guo, Y., Shen, H., Huang, D. D., Zhang, Y., and Zhao, D.: Effect of relative humidity on the
919 molecular composition of secondary organic aerosols from α-pinene ozonolysis, Environmental
920 Science: Atmospheres, 10.1039/D3EA00149K, 2024.
921 Mermet, K., Perraudin, E., Dusanter, S., Sauvage, S., Léonardis, T., Flaud, P.-M., Bsaibes, S., Kammer,
922 J., Michoud, V., Gratien, A., Cirtog, M., Al Ajami, M., Truong, F., Batut, S., Hecquet, C., Doussin,
923 J.-F., Schoemaecker, C., Gros, V., Locoge, N., and Villenave, E.: Atmospheric reactivity of biogenic
924 volatile organic compounds in a maritime pine forest during the LANDEX episode 1 field campaign,
925 Sci. Total Environ., 756, 144129, https://doi.org/10.1016/j.scitotenv.2020.144129, 2021.
926 Mohr, C., Lopez-Hilfiker, F. D., Yli-Juuti, T., Heitto, A., Lutz, A., Hallquist, M., D'Ambro, E. L.,
927 Rissanen, M. P., Hao, L., Schobesberger, S., Kulmala, M., Mauldin III, R. L., Makkonen, U., Sipilä,
928 M., Petäjä, T., and Thornton, J. A.: Ambient observations of dimers from terpene oxidation in the
929 gas phase: Implications for new particle formation and growth, Geophys. Res. Lett., 44, 2958-2966,
930 https://doi.org/10.1002/2017GL072718, 2017.
931 Muller, M., Eicher, P., D'Anna, B., Tan, W., and Wisthaler, A.: Direct Sampling and Analysis of
932 Atmospheric Particulate Organic Matter by Proton-Transfer-Reaction Mass Spectrometry,
933 Analytical Chemistry, 89, 10889-10897, 10.1021/acs.analchem.7b02582, 2017.
934 Müller, M., Eichler, P., D'Anna, B., Tan, W., and Wisthaler, A.: Direct Sampling and Analysis of
935 Atmospheric Particulate Organic Matter by Proton-Transfer-Reaction Mass Spectrometry, Anal.
936 Chem., 89, 10889-10897, 10.1021/acs.analchem.7b02582, 2017.
937 Ng, N. L., Canagaratna, M. R., Jimenez, J. L., Chhabra, P. S., Seinfeld, J. H., and Worsnop, D. R.:
938 Changes in organic aerosol composition with aging inferred from aerosol mass spectra, Atmos.
939 Chem. Phys., 11, 6465-6474, 10.5194/acp-11-6465-2011, 2011.
940 Ng, N. L., Canagaratna, M. R., Zhang, Q., Jimenez, J. L., Tian, J., Ulbrich, I. M., Kroll, J. H., Docherty,
941 K. S., Chhabra, P. S., Bahreini, R., Murphy, S. M., Seinfeld, J. H., Hildebrandt, L., Donahue, N. M.,
942 DeCarlo, P. F., Lanz, V. A., Prevot, A. S. H., Dinar, E., Rudich, Y., and Worsnop, D. R.: Organic
943 aerosol components observed in Northern Hemispheric datasets from Aerosol Mass Spectrometry,
944 Atmos. Chem. Phys., 10, 4625-4641, 10.5194/acp-10-4625-2010, 2010.
945 Paatero, P. and Tapper, U.: Positive matrix factorization: A non-negative factor model with optimal
946 utilization of error estimates of data values, Environmetrics, 5, 111-126,
947 https://doi.org/10.1002/env.3170050203, 1994.
948 Pagonis, D., Sekimoto, K., and de Gouw, J.: A Library of Proton-Transfer Reactions of H3O+ Ions Used
949 for Trace Gas Detection, Journal of the American Society for Mass Spectrometry, 30, 1330-1335,
950 10.1007/s13361-019-02209-3, 2019.
951 Papurello, D., Soukoulis, C., Schuhfried, E., Cappellin, L., Gasperi, F., Silvestri, S., Santarelli, M., and
952 Biasioli, F.: Monitoring of volatile compound emissions during dry anaerobic digestion of the
953 Organic Fraction of Municipal Solid Waste by Proton Transfer Reaction Time-of-Flight Mass
954 Spectrometry, Bioresource Technology, 126, 254-265,
955 https://doi.org/10.1016/j.biortech.2012.09.033, 2012.
956 Peng, Y., Wang, H., Gao, Y., Jing, S., Zhu, S., Huang, D., Hao, P., Lou, S., Cheng, T., Huang, C., and
957 Zhang, X.: Real-time measurement of phase partitioning of organic compounds using a proton-
958 transfer-reaction time-of-flight mass spectrometer coupled to a CHARON inlet, Atmos. Meas.
959 Tech., 16, 15-28, 10.5194/amt-16-15-2023, 2023.
960 Peñuelas, J. and Staudt, M.: BVOCs and global change, Trends Plant Sci., 15, 133-144, 2010.
961 Pernov, J. B., Bossi, R., Lebourgeois, T., Nøjgaard, J. K., Holzinger, R., Hjorth, J. L., and Skov, H.:
962 Atmospheric VOC measurements at a High Arctic site: characteristics and source apportionment,
963 Atmos. Chem. Phys., 21, 2895-2916, 10.5194/acp-21-2895-2021, 2021.
964 Peron, A., Kaser, L., Fitzky, A. C., Graus, M., Halbwirth, H., Greiner, J., Wohlfahrt, G., Rewald, B.,
965 Sandén, H., and Karl, T.: Combined effects of ozone and drought stress on the emission of biogenic

volatile organic compounds from Quercus robur L, Biogeosciences, 18, 535-556, 10.5194/bg-18-535-2021, 2021.
Piel, F., Müller, M., Winkler, K., Skytte af Sätra, J., and Wisthaler, A.: Introducing the extended volatility range proton-transfer-reaction mass spectrometer (EVR PTR-MS), Atmos. Meas. Tech., 14, 1355-1363, 10.5194/amt-14-1355-2021, 2021.
Rasmussen, R. A. and Went, F.: Volatile organic material of plant origin in the atmosphere, Proc. Natl. Acad. Sci. U.S.A., 53, 215-220, 1965.
Salazar Gómez, J. I., Lohmann, H., and Krassowski, J.: Determination of volatile organic compounds from biowaste and co-fermentation biogas plants by single-sorbent adsorption, Chemosphere, 153, 48-57, https://doi.org/10.1016/j.chemosphere.2016.02.128, 2016.
Scheftelowitz, M., Becker, R., and Thrän, D.: Improved power provision from biomass: A retrospective on the impacts of German energy policy, Biomass and Bioenergy, 111, 1-12, https://doi.org/10.1016/j.biombioe.2018.01.010, 2018.
Shrivastava, M., Cappa, C. D., Fan, J., Goldstein, A. H., Guenther, A. B., Jimenez, J. L., Kuang, C., Laskin, A., Martin, S. T., Ng, N. L., Petaja, T., Pierce, J. R., Rasch, P. J., Roldin, P., Seinfeld, J. H., Shilling, J., Smith, J. N., Thornton, J. A., Volkamer, R., Wang, J., Worsnop, D. R., Zaveri, R. A., Zelenyuk, A., and Zhang, Q.: Recent advances in understanding secondary organic aerosol: Implications for global climate forcing, Reviews of Geophysics, 55, 509-559, https://doi.org/10.1002/2016RG000540, 2017.
Sindelarova, K., Granier, C., Bouarar, I., Guenther, A., Tilmes, S., Stavrakou, T., Müller, J. F., Kuhn, U., Stefani, P., and Knorr, W.: Global data set of biogenic VOC emissions calculated by the MEGAN model over the last 30 years, Atmos. Chem. Phys., 14, 9317-9341, 10.5194/acp-14-9317-2014, 2014.
Smiatek, G. and Steinbrecher, R.: Temporal and spatial variation of forest VOC emissions in Germany in the decade 1994–2003, Atmos. Environ., 40, 166-177, https://doi.org/10.1016/j.atmosenv.2005.11.071, 2006.
Song, J., Saathoff, H., Jiang, F., Gao, L., Zhang, H., and Leisner, T.: Sources of organic gases and aerosol particles and their roles in nighttime particle growth at a rural forested site in southwest Germany, Atmos. Chem. Phys., 24, 6699-6717, 10.5194/acp-24-6699-2024, 2024.
Song, J., Saathoff, H., Gao, L., Gebhardt, R., Jiang, F., Vallon, M., Bauer, J., Norra, S., and Leisner, T.: Variations of PM2.5 sources in the context of meteorology and seasonality at an urban street canyon in Southwest Germany, Atmos. Environ., 119147, https://doi.org/10.1016/j.atmosenv.2022.119147, 2022.
Surdu, M., Lamkaddam, H., Wang, D. S., Bell, D. M., Xiao, M., Lee, C. P., Li, D., Caudillo, L., Marie, G., Scholz, W., Wang, M., Lopez, B., Piedehierro, A. A., Ataei, F., Baalbaki, R., Bertozzi, B., Bogert, P., Brasseur, Z., Dada, L., Duplissy, J., Finkenzeller, H., He, X.-C., Höhler, K., Korhonen, K., Krechmer, J. E., Lehtipalo, K., Mahfouz, N. G. A., Manninen, H. E., Marten, R., Massabò, D., Mauldin, R., Petäjä, T., Pfeifer, J., Philippov, M., Rörup, B., Simon, M., Shen, J., Umo, N. S., Vogel, F., Weber, S. K., Zauner-Wieczorek, M., Volkamer, R., Saathoff, H., Möhler, O., Kirkby, J., Worsnop, D. R., Kulmala, M., Stratmann, F., Hansel, A., Curtius, J., Welti, A., Riva, M., Donahue, N. M., Baltensperger, U., and El Haddad, I.: Molecular Understanding of the Enhancement in Organic Aerosol Mass at High Relative Humidity, Environ. Sci. Technol., 57, 2297-2309, 10.1021/acs.est.2c04587, 2023.
Tani, A., Hayward, S., and Hewitt, C. N.: Measurement of monoterpenes and related compounds by proton transfer reaction-mass spectrometry (PTR-MS), International Journal of Mass Spectrometry, 223-224, 561-578, https://doi.org/10.1016/S1387-3806(02)00880-1, 2003.
Teskey, R., Wertin, T., Bauweraerts, I., Ameye, M., McGuire, M. A., and Steppe, K.: Responses of tree species to heat waves and extreme heat events, Plant, Cell & Environment, 38, 1699-1712, https://doi.org/10.1111/pce.12417, 2015.
Tillmann, R., Hallquist, M., Jonsson, Å. M., Kiendler-Scharr, A., Saathoff, H., Iinuma, Y., and Mentel, T. F.: Influence of relative humidity and temperature on the production of pinonaldehyde and OH radicals from the ozonolysis of α-pinene, Atmos. Chem. Phys., 10, 7057-7072, 10.5194/acp-10-7057-2010, 2010.

Trainer, M., Williams, E. J., Parrish, D. D., Buhr, M. P., Allwine, E. J., Westberg, H. H., Fehsenfeld, F. C., and Liu, S. C.: Models and observations of the impact of natural hydrocarbons on rural ozone, Nature, 329, 705-707, 10.1038/329705a0, 1987.

van Meeningen, Y., Schurgers, G., Rinnan, R., and Holst, T.: Isoprenoid emission response to changing light conditions of English oak, European beech and Norway spruce, Biogeosciences, 14, 4045-4060, 10.5194/bg-14-4045-2017, 2017.

Vermeuel, M. P., Novak, G. A., Kilgour, D. B., Claflin, M. S., Lerner, B. M., Trowbridge, A. M., Thom, J., Cleary, P. A., Desai, A. R., and Bertram, T. H.: Observations of biogenic volatile organic compounds over a mixed temperate forest during the summer to autumn transition, Atmos. Chem. Phys., 23, 4123-4148, 10.5194/acp-23-4123-2023, 2023.

Vestenius, M., Hopke, P. K., Lehtipalo, K., Petäjä, T., Hakola, H., and Hellén, H.: Assessing volatile organic compound sources in a boreal forest using positive matrix factorization (PMF), Atmos. Environ., 259, 118503, https://doi.org/10.1016/j.atmosenv.2021.118503, 2021.

von Hessberg, C., von Hessberg, P., Pöschl, U., Bilde, M., Nielsen, O. J., and Moortgat, G. K.: Temperature and humidity dependence of secondary organic aerosol yield from the ozonolysis of β-pinene, Atmos. Chem. Phys., 9, 3583-3599, 10.5194/acp-9-3583-2009, 2009.

Wang, L., Slowik, J. G., Tripathi, N., Bhattu, D., Rai, P., Kumar, V., Vats, P., Satish, R., Baltensperger, U., Ganguly, D., Rastogi, N., Sahu, L. K., Tripathi, S. N., and Prévôt, A. S. H.: Source characterization of volatile organic compounds measured by proton-transfer-reaction time-of-flight mass spectrometers in Delhi, India, Atmos. Chem. Phys., 20, 9753-9770, 10.5194/acp-20-9753-2020, 2020.

Weber, J., Archer-Nicholls, S., Abraham, N. L., Shin, Y. M., Griffiths, P., Grosvenor, D. P., Scott, C. E., and Archibald, A. T.: Chemistry-driven changes strongly influence climate forcing from vegetation emissions, Nature Communications, 13, 7202, 10.1038/s41467-022-34944-9, 2022.

Wennberg, P. O., Bates, K. H., Crounse, J. D., Dodson, L. G., McVay, R. C., Mertens, L. A., Nguyen, T. B., Praske, E., Schwantes, R. H., Smarte, M. D., St Clair, J. M., Teng, A. P., Zhang, X., and Seinfeld, J. H.: Gas-Phase Reactions of Isoprene and Its Major Oxidation Products, Chem Rev, 118, 3337-3390, 10.1021/acs.chemrev.7b00439, 2018.

Wu, R., Pan, S., Li, Y., and Wang, L.: Atmospheric Oxidation Mechanism of Toluene, The Journal of Physical Chemistry A, 118, 4533-4547, 10.1021/jp500077f, 2014.

Yáñez-Serrano, A. M., Bach, A., Bartolomé-Català, D., Matthaios, V., Seco, R., Llusià, J., Filella, I., and Peñuelas, J.: Dynamics of volatile organic compounds in a western Mediterranean oak forest, Atmos. Environ., 257, 118447, https://doi.org/10.1016/j.atmosenv.2021.118447, 2021.

Yáñez-Serrano, A. M., Bourtsoukidis, E., Alves, E. G., Bauwens, M., Stavrakou, T., Llusià, J., Filella, I., Guenther, A., Williams, J., Artaxo, P., Sindelarova, K., Doubalova, J., Kesselmeier, J., and Peñuelas, J.: Amazonian biogenic volatile organic compounds under global change, Global Change Biology, 26, 4722-4751, https://doi.org/10.1111/gcb.15185, 2020.

Yatavelli, R. L. N., Stark, H., Thompson, S. L., Kimmel, J. R., Cubison, M. J., Day, D. A., Campuzano-Jost, P., Palm, B. B., Hodzic, A., Thornton, J. A., Jayne, J. T., Worsnop, D. R., and Jimenez, J. L.: Semicontinuous measurements of gas–particle partitioning of organic acids in a ponderosa pine forest using a MOVI-HRToF-CIMS, Atmos. Chem. Phys., 14, 1527-1546, 10.5194/acp-14-1527-2014, 2014.

Zaytsev, A., Koss, A. R., Breitenlechner, M., Krechmer, J. E., Nihill, K. J., Lim, C. Y., Rowe, J. C., Cox, J. L., Moss, J., Roscioli, J. R., Canagaratna, M. R., Worsnop, D. R., Kroll, J. H., and Keutsch, F. N.: Mechanistic study of the formation of ring-retaining and ring-opening products from the oxidation of aromatic compounds under urban atmospheric conditions, Atmos. Chem. Phys., 19, 15117-15129, 10.5194/acp-19-15117-2019, 2019.

Zhang, X., McVay, R. C., Huang, D. D., Dalleska, N. F., Aumont, B., Flagan, R. C., and Seinfeld, J. H.: Formation and evolution of molecular products in α-pinene secondary organic aerosol, Proceedings of the National Academy of Sciences, 112, 14168-14173, doi:10.1073/pnas.1517742112, 2015.

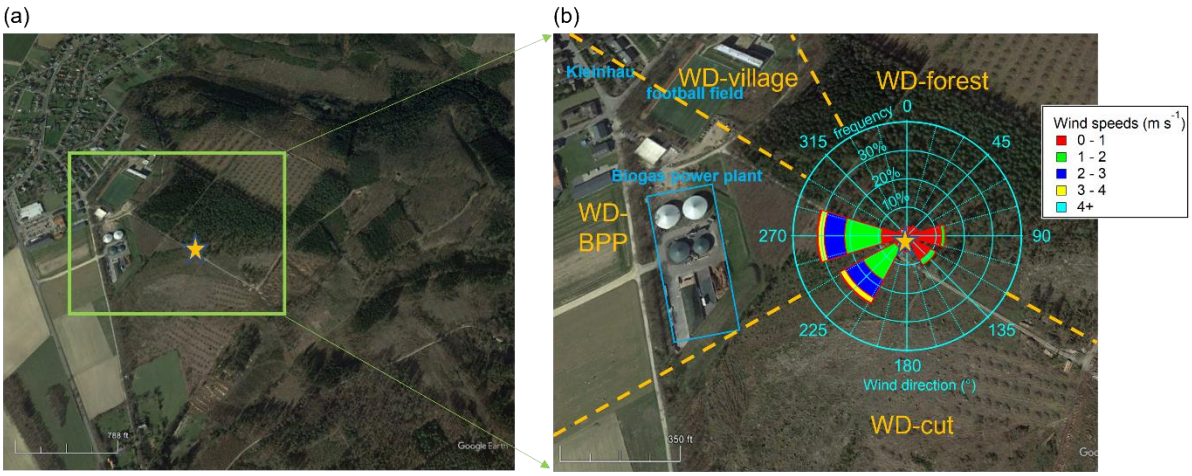

1072

1073 **Figure 1.** (a) Location of the sampling site (orange star) (©Google Earth); (b) a close look at
1074 sampling site with the centered wind rose for the entire measurement period. The orange dash
1075 lines are shown for distinguishing different sectors of wind direction (WD). The WD-forest of
1076 0-120º is influenced by an intact forest area, the WD-cut of 120-240º is influenced by a clear-
1077 cut area, the WD-BPP of 240-300º is influenced by a biogas power plant (blue rectangle) and
1078 the WD-village of 300-330º is influenced by the residential areas of Kleinhau.

1079

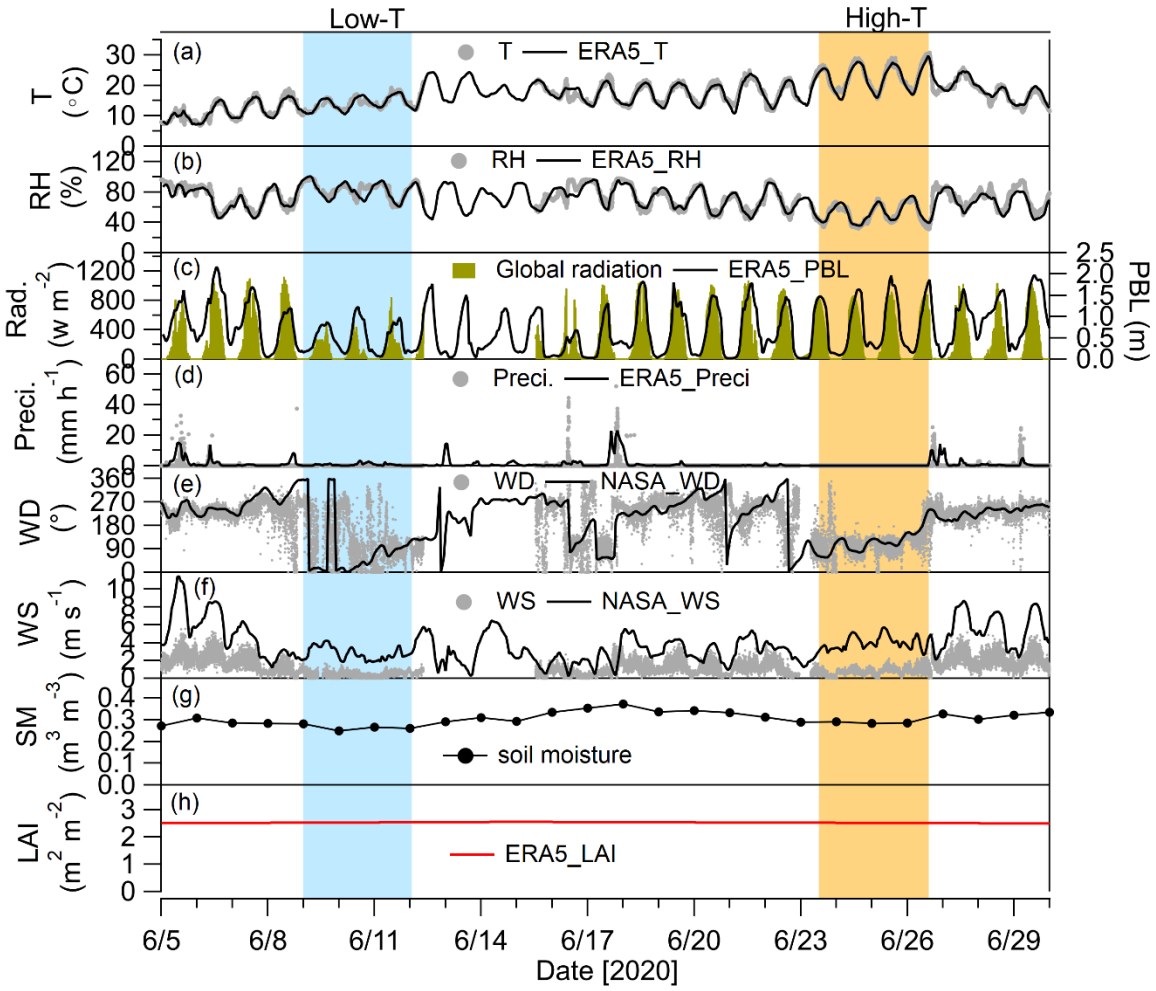

Figure 2. (a-f) Time series of meteorological data measured at the sampling site with hourly data of temperature (T), relative humidity (RH), precipitation (Preci.) and planetary boundary layer (PBL) height obtained from ERA5 reanalysis (Hersbach et al., 2020) and hourly data of wind direction and speed (WD and WS) obtained from NASA Power Data Access Viewer (power.larc.nasa.gov); (g) daily soil moisture (SM) measured by a cosmic ray neutron sensor which was located ~ 150 m southwest of the sampling site; and (h) leaf area index (LAI) obtained from ERA5 reanalysis. The blue and yellow shaded areas mark the low-T and high-T episodes.

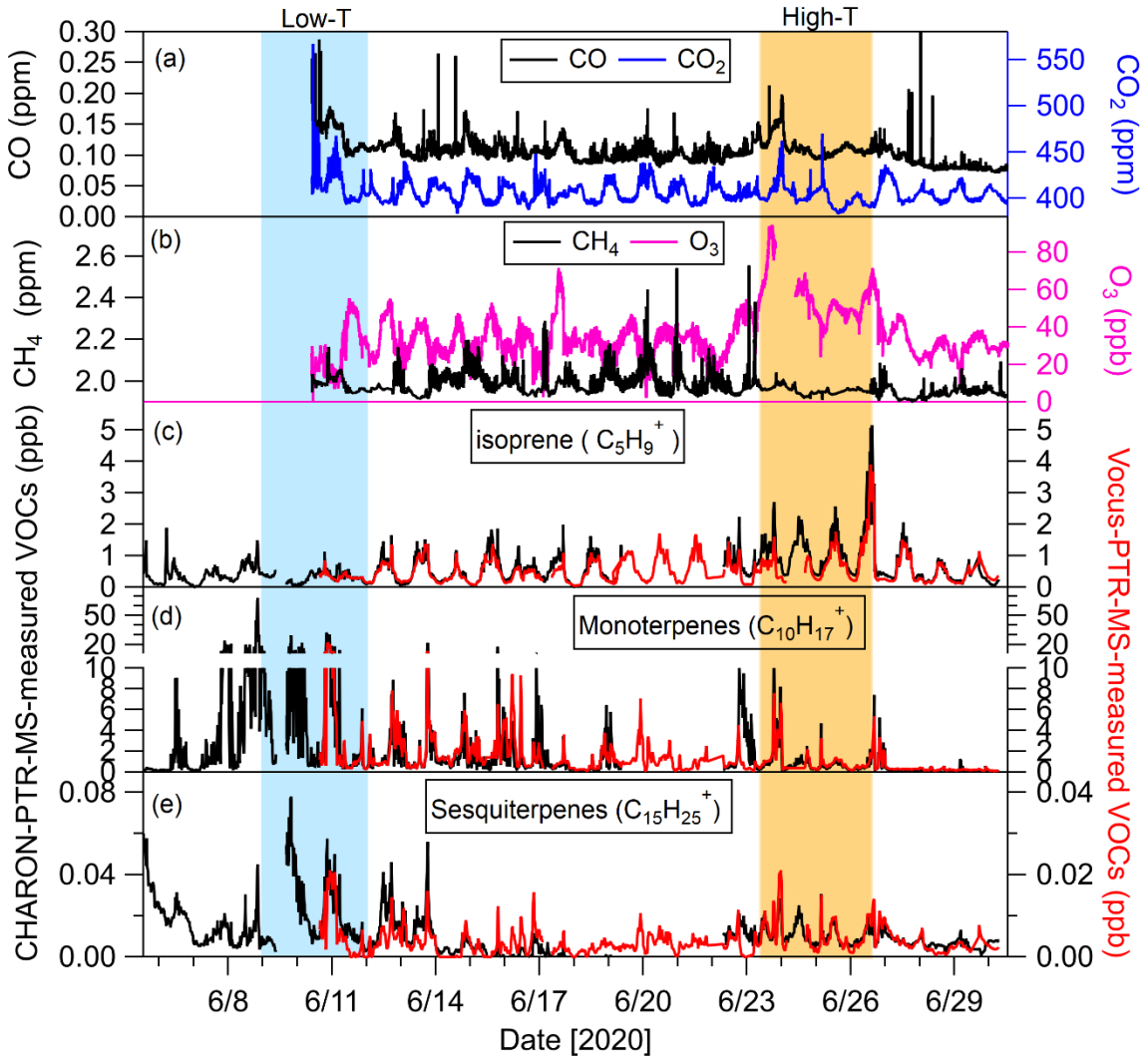

1089

1090 **Figure 3.** Time series of gas concentrations: (a) CO and CO_2; (b) CH_4 and O_3; (c-e) isoprene,
1091 monoterpenes, sesquiterpenes measured by the CHARON-PTR-MS (black lines) and Vocus-
1092 PTR-MS (red lines) respectively. The blue and yellow shaded areas mark the low-T and high-
1093 T episodes.

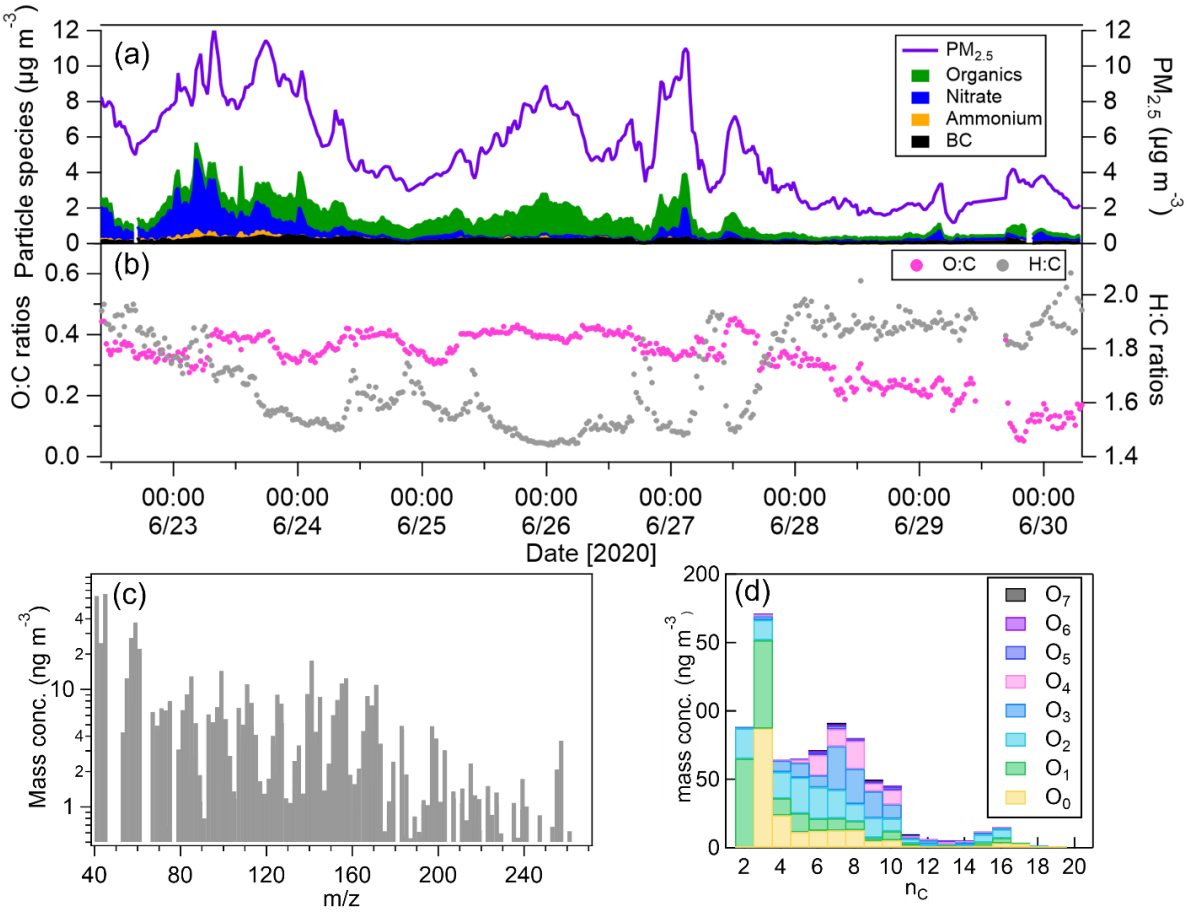

1094

1095 **Figure 4.** Time series of (a) mass concentrations of $PM_{2.5}$, BC and semi-volatile particle species
1096 (organics, nitrate and ammonium) measured by the CHARON-PTR-ToF-MS simultaneously
1097 available during 22nd-30th June; (b) oxygen to carbon (O:C) and hydrogen to carbon (H:C) ratios
1098 of organics. (c) average mass spectrum of organics; (d) mass distributions of organics associated
1099 with $C_xH_yO_{0\text{-}7}^+$ resolved by the carbon and oxygen numbers (n_C and n_O).

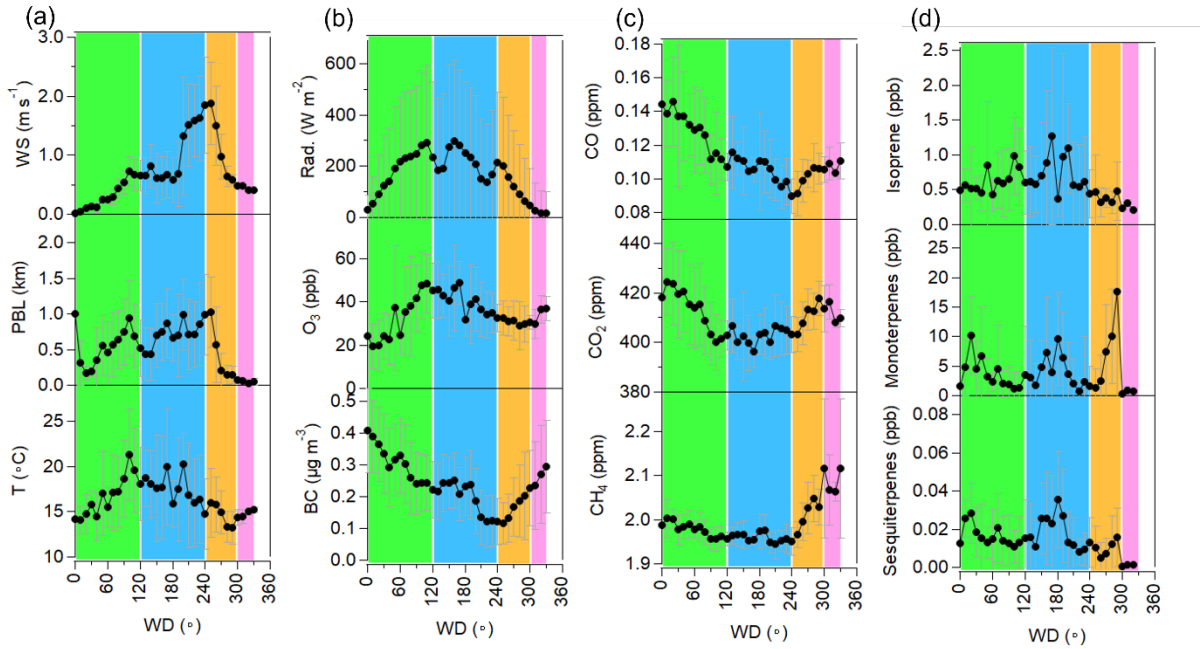

Figure 5. Variations of (a) wind speed (WS), planetary boundary layer (PBL) and ambient temperature; (b) global radiation, O_3 and BC mass concentrations; (c) mixing ratios of CO, CO_2 and CH_4 and (d) mixing ratios of isoprene, monoterpenes and sesquiterpenes as a function of wind direction (WD). The black dots and whiskers represent the mean values and standard deviations in each WD bin of 10º. Data within the WD1 of 0-120º is influenced by an intact forest area (light green), the WD2 of 120-240º is influenced by a clear-cut area (light blue), the WD3 of 240-300º is influenced by a biogas power plant (yellow) and the WD4 of 300-330º is influenced by the village (pink).

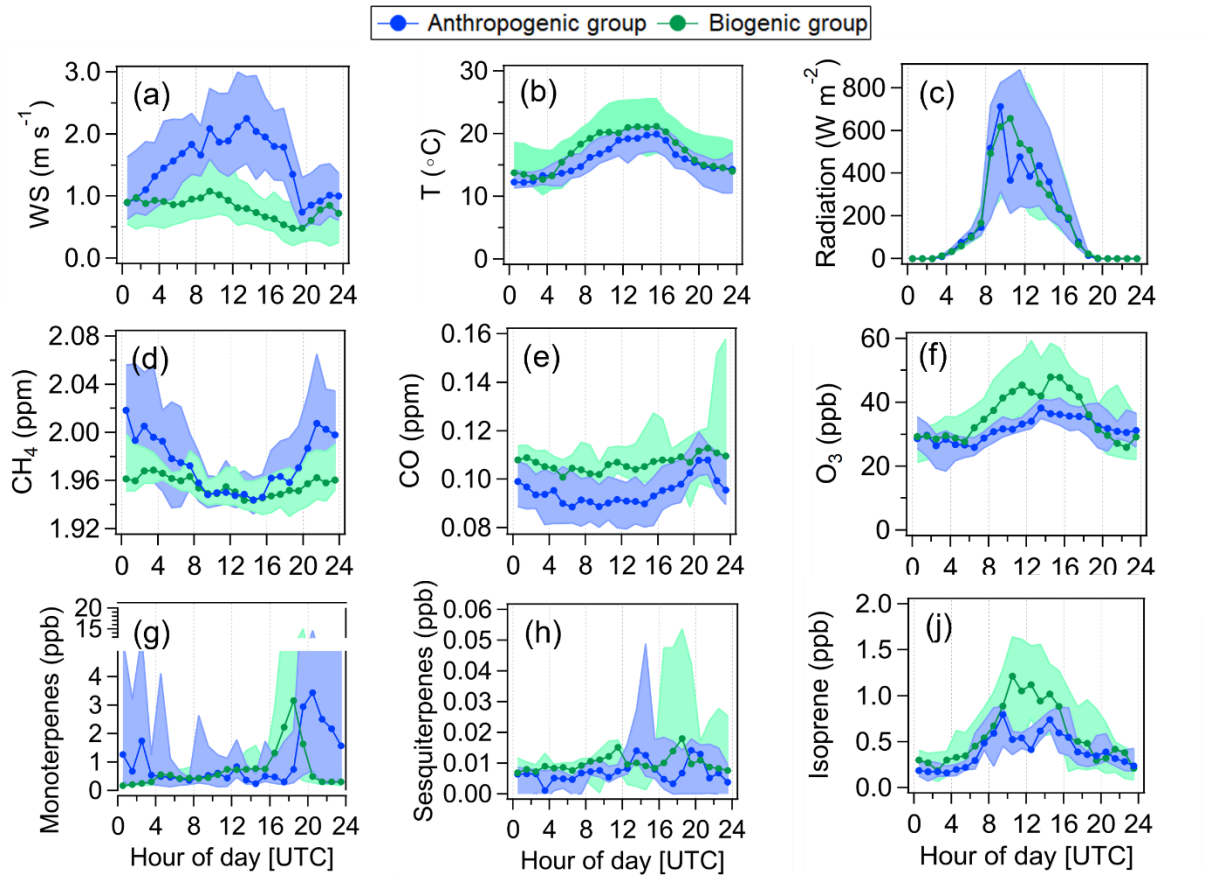

1109

1110 **Figure 6.** Diurnal variations of (a-c) wind speeds, ambient temperature and global radiation;
1111 (d-f) CH_4, CO and O_3; (g-j) monoterpenes, sesquiterpenes and isoprene. The blue and green
1112 markers represent the median values for the anthropogenic-group and biogenic-group, which
1113 were calculated from the data within the sectors of WD-forest and WD-cut, and WD-BPP and
1114 WD-village, respectively. The shaded areas represent the 25th and 75th percentiles.

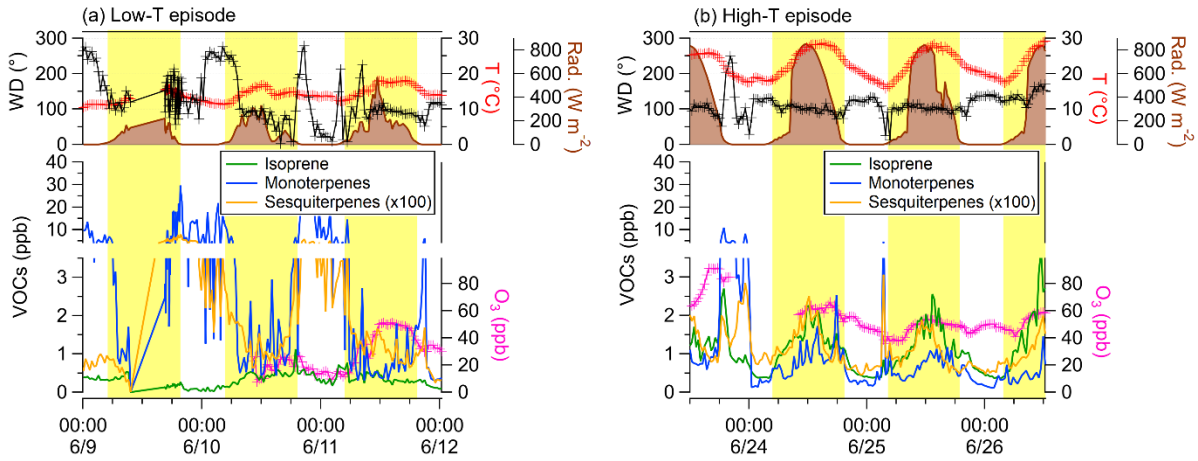

Figure 7. Time series of wind direction, ambient temperature, global radiation, isoprene, monoterpenes, sesquiterpenes and O_3 during the low-T episode (a) and high-T episode (b). The yellow shaded areas mark the daytime from 4:00-20:00 UTC.

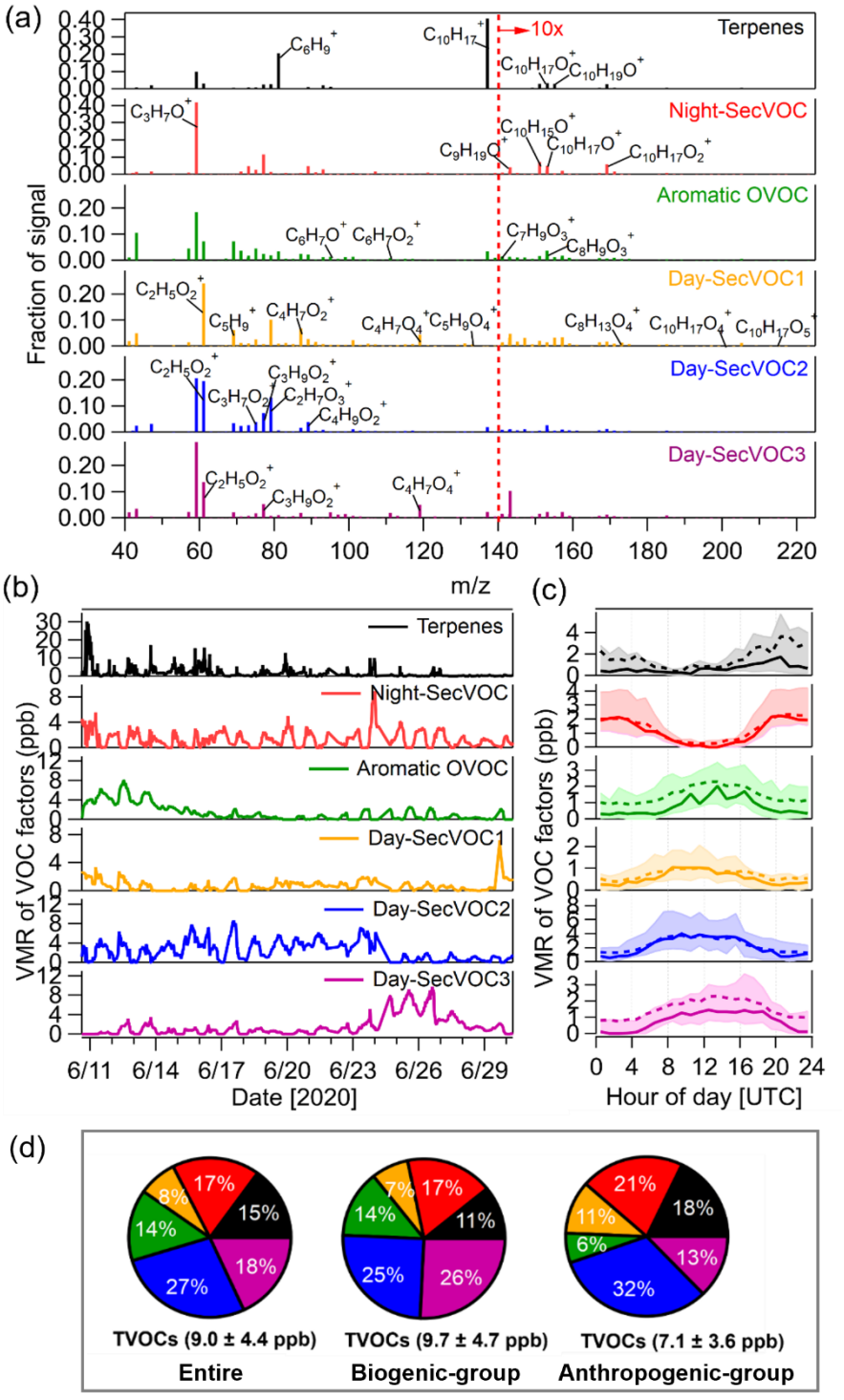

1121

1122 **Figure 8.** (a) Factor profiles of six VOC factors resolved from the PMF analysis of Vocus-PTR-
1123 ToF-MS data. The fraction of signal at high mass range (*m/z*140-230) is scaled by a factor of
1124 10; (b) time series of six VOC factors; (c) diurnal variations of six VOC factors during the entire
1125 measurement campaign. The solid and dash lines represent median and mean values
1126 respectively and the shaded areas represent the 25th and 75th percentiles. (d) Average
1127 contributions of six VOC factors to TVOCs for the entire measurement campaign and the
1128 biogenic-group and anthropogenic-group.

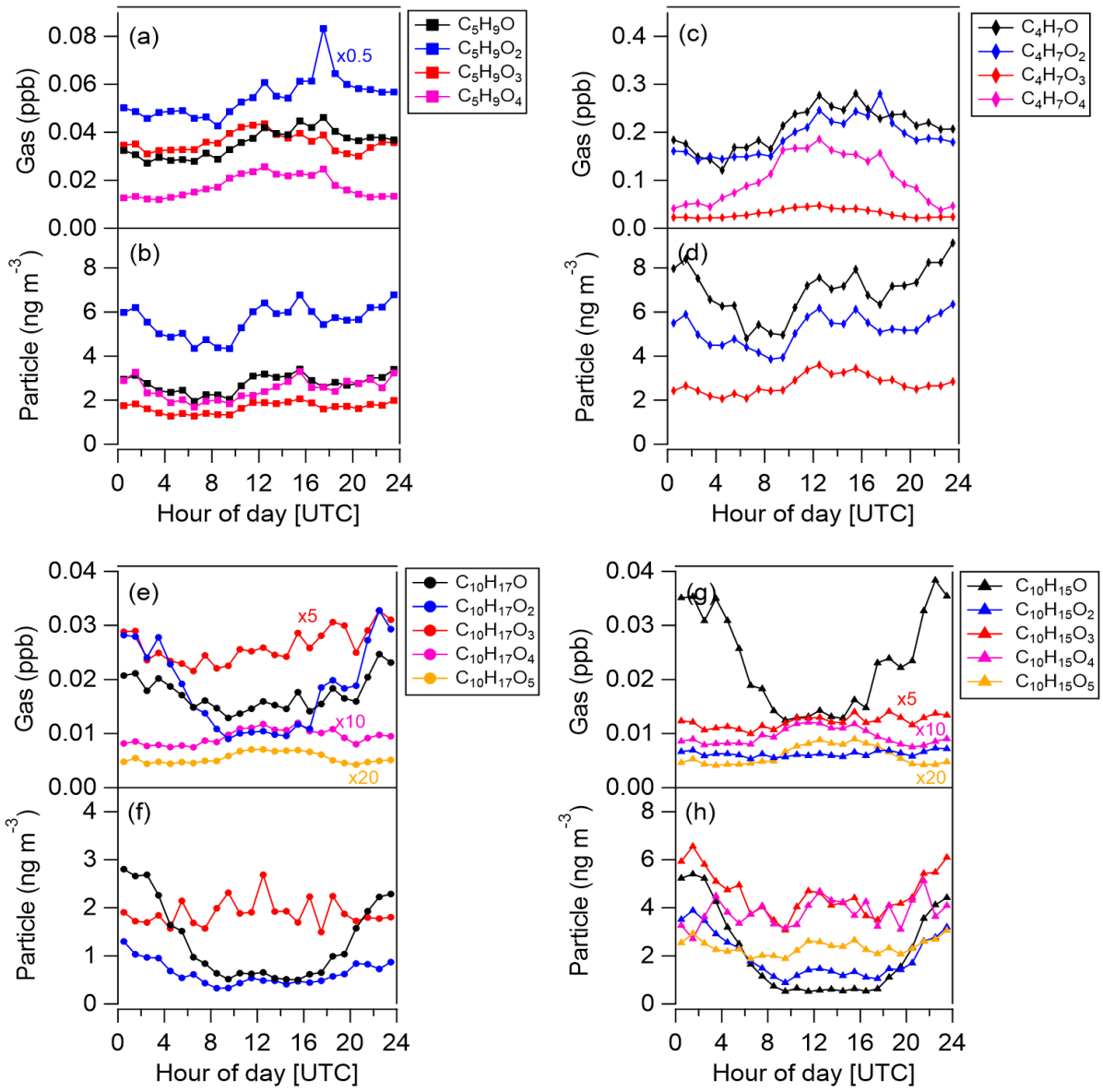

1129

1130 **Figure 9.** Diurnal variations of (a-d) concentrations of isoprene oxidation products ($C_5H_9O_{1\text{-}4}^+$
1131 and $C_4H_7O_{1\text{-}4}^+$) in gas and particle phases; (e-h) concentrations of monoterpene oxidation
1132 products ($C_{10}H_{17}O_{1\text{-}5}^+$ and $C_{10}H_{15}O_{1\text{-}5}^+$) in gas and particle phases calculated for the
1133 measurement period of 22nd-30th of June. Gas- and particle-phase data were taken from the
1134 Vocus-PTR-ToF-MS and CHARON-PTR-ToF-MS measurements, respectively. The higher-
1135 oxidized particle-phase products from isoprene ($C_4H_7O_4^+$) and monoterpenes ($C_{10}H_{17}O_{4\text{-}5}^+$)
1136 cannot be detected by the CHARON-PTR-ToF-MS.

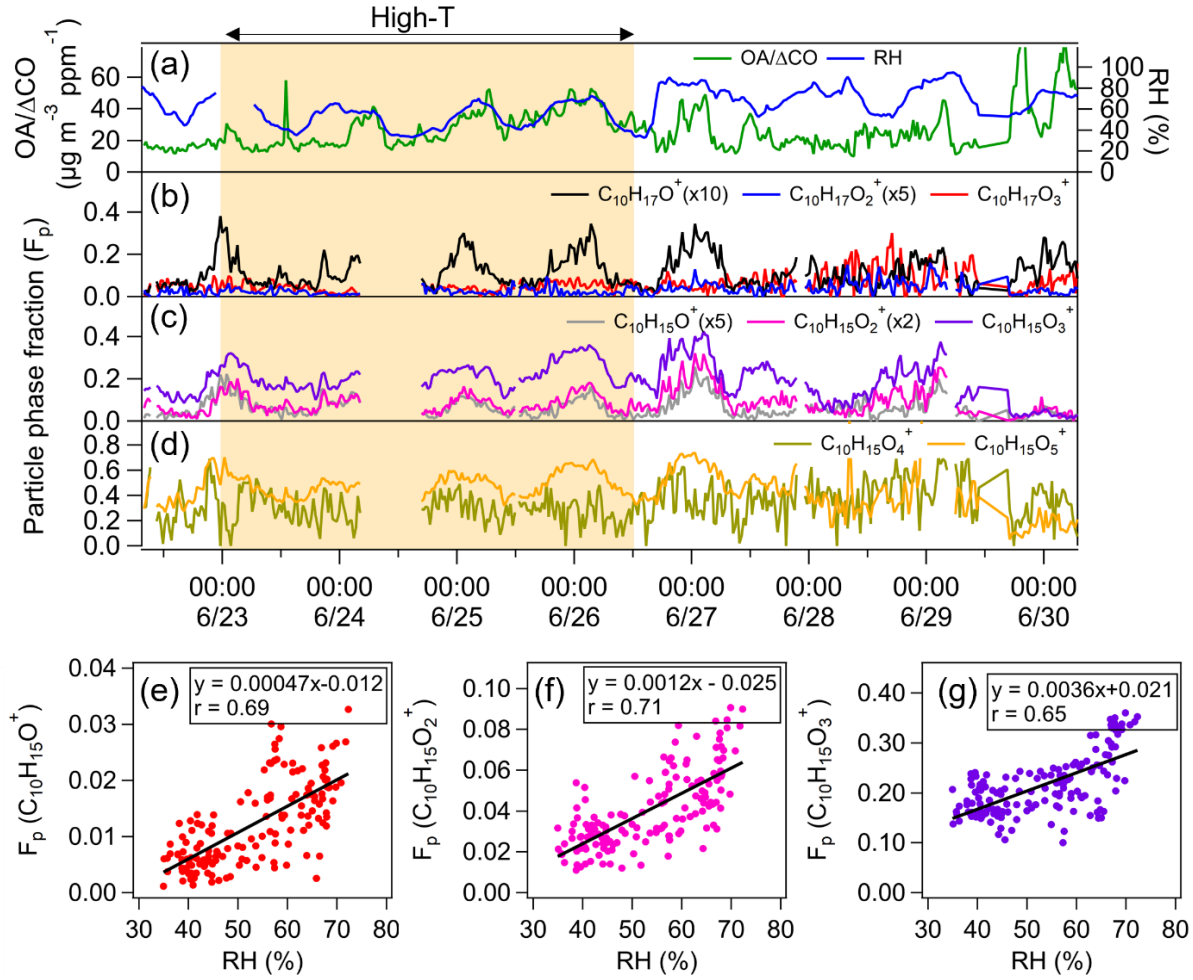

Figure 10. Time series of (a) OA/ΔCO and relative humidity (RH); (b-d) particle phase fraction of monoterpene oxidation products ($C_{10}H_{17}O_{1\text{-}3}^{+}$ and $C_{10}H_{15}O_{1\text{-}5}^{+}$) from 22nd-30th of June. The yellow shaded area marks the high-T episode. (e-f) Correlations of the time series of particle phase fraction of $C_{10}H_{15}O_{1\text{-}3}^{+}$ with RH during high-T episode.